NATO STANDARD

AEP-4655

AN ENGINEERING MODEL TO ESTIMATE AERODYNAMIC COEFFICIENTS

Edition A Version 1

NOVEMBER 2016

NORTH ATLANTIC TREATY ORGANIZATION

ALLIED ENGINEERING PUBLICATION

Published by the
NATO STANDARDIZATION OFFICE (NSO)

INTENTIONALLY BLANK

NORTH ATLANTIC TREATY ORGANIZATION (NATO)

NATO STANDARDIZATION OFFICE (NSO)

NATO LETTER OF PROMULGATION

10 November 2016

1. The enclosed Allied Engineering Publication AEP-4655, Edition A, Version 1 AN ENGINEERING MODEL TO ESTIMATE AERODYNAMIC COEFFICIENTS, which has been approved by the nations in the, AC/225 - NATO Army Armaments Group, is promulgated herewith. The recommendation of nations to use this publication is recorded in STANREC 4655.

2. AEP-4655, Edition A, Version 1 is effective upon receipt.

4. This publication shall be handled in accordance with C-M(2002)60.

Edvardas MAZEIKIS
Major General, LTUAF
Director NATO Standardization Office

INTENTIONALLY BLANK

RESERVED FOR NATIONAL LETTER OF PROMULGATION

INTENTIONALLY BLANK

RECORD OF RESERVATIONS

CHAPTER	RECORD OF RESERVATION BY NATIONS

Note: The reservations listed on this page include only those that were recorded at time of promulgation and may not be complete. Refer to the NATO Standardization Document Database for the complete list of existing reservations.

INTENTIONALLY BLANK

RECORD OF SPECIFIC RESERVATIONS

[nation]	[detail of reservation]
Note: The reservations listed on this page include only those that were recorded at time of promulgation and may not be complete. Refer to the NATO Standardization Document Database for the complete list of existing reservations.	

INTENTIONALLY BLANK

TABLE OF CONTENTS

CHAPTER 1 BODY AERODYNAMICS

1.1 DRAG COMPUTATION

1. The zero angle of attack drag of a projectile consists of the pressure drag of the nose, boat-tail/flare, tail boom, base, protuberances (driving band, grooves and steps), nubs and of the viscous drag as a sum of the following form:

$$C_{D_0} = C_{D_n} + C_{D_{FL}} + C_{D_{bt}} + C_{D_b} + C_{D_{pr}} + C_{D_{Nubs}} + C_{D_f} \quad \text{1-1}$$

2. The detailed methods to determine the coefficients for pressure drag components and viscous drag are presented in the **Annex B**.

1.2 LIFT FORCE COMPUTATION

1. The zero lift force coefficient slope is derived from computed normal force coefficient slope and zero angle of attack drag

$$C_{L_{\alpha_0}} = C_{N_{\alpha_0}} - C_{D_0} \quad \text{1-2}$$

2. The zero normal force coefficient slope is obtained as a sum of the component slopes

$$C_{N_{\alpha_0}} = C_{N_{\alpha_{n_0}}} + C_{N_{\alpha_{b_0}}} + \Delta C_{N_{\alpha_0}} \quad \text{1-3}$$

3. The components $C_{N_{\alpha_{n_0}}}$, $C_{N_{\alpha_{b_0}}}$ and $\Delta C_{N_{\alpha_0}}$ are the nose normal force coefficient slope, the body normal force coefficient slope and the change of the normal force coefficient slope due to the boat-tail or flare (including possible tail boom) respectively.

4. The detailed methods to determine the lift force coefficient slope are presented in the **Annex C**.

1.3 MOMENT COMPUTATIONS

1. The zero pitching moment coefficient slope is obtained as a sum of the component slopes

$$C_{m_{\alpha_0}} = C_{m_{\alpha_{n_0}}} + C_{m_{\alpha_{b_0}}} + \Delta C_{m_{\alpha_0}} \quad \text{1-4}$$

2. The components $C_{m_{\alpha_{n_0}}}$, $C_{m_{\alpha_{b_0}}}$ and $\Delta C_{m_{\alpha_0}}$ are the nose pitching moment coefficient slope, the body pitching moment coefficient slope and the change of the pitching moment coefficient slope due to the boat-tail or flare (including possible tail boom) respectively.

3. The sum of pitch damping moment coefficients is computed from

$$C_{m_q} + C_{m_{\dot{\alpha}}} = -2C_{N_\alpha}\left(\frac{l}{d}\right)^2\left(l_{eff} - \frac{x_{cg}}{l}\right)^2 \quad \text{1-5}$$

4. The Magnus force coefficient slope $C_{Y_{p\alpha}}$ is computed from

$$C_{Y_{p\alpha}} = k(Ma)\frac{V_B}{5d_b^3} \quad \text{1-6}$$

5. The Magnus moment coefficient slope is computed from

$$C_{n_{p\alpha}} = C_{Y_{p\alpha}}\frac{\left(x_{cg} - x_{forcecenter}\right)}{d} \quad \text{1-7}$$

6. The detailed methods to determine the pitching moment coefficient slope $C_{m_{\alpha_0}}$, the pitch damping moment $C_{m_q} + C_{m_{\dot{\alpha}}}$, the Magnus force coefficient slope $C_{Y_{p\alpha}}$ and the Magnus moment coefficient slope $C_{n_{p\alpha}}$ are presented in the **Annex C**.

CHAPTER 2 FIN AERODYNAMICS

2.1 DRAG COMPUTATION

1. The zero angle of attack drag of a projectile consists of the individuals drags of projectile body and fins. The corresponding drag coefficient C_{D_0} can be written as a sum of the following form:

$$C_{D_0} = C_{D_{body}} + C_{D_{fin}} \qquad 2\text{-}1$$

2. This chapter describes a simplified method to compute the drag coefficient of fins $C_{D_{fin}}$. The computation method for obtaining drag coefficient $C_{D_{body}}$ is discussed in Chapter 1.

2. The drag coefficient of fins $C_{D_{fin}}$ at zero angle of attack is computed from

$$C_{D_{fin}} = C_{D_{fin_{viscous}}} + C_{D_{fin_{wave}}} + C_{D_{fin_{LE}}} + C_{D_{fin_{TE}}} \qquad 2\text{-}2$$

The subscripts LE and TE are for leading edge and trailing edge respectively.

3. The detailed methods to determine the coefficients for drag components are presented in **Annex D**.

2.2 LIFT FORCE COMPUTATION

1. The lift and pitching moment for a fin-stabilized projectile are obtained by summing the body and fins contributions. The methods to estimate the body lift are described in Part I.

2. The projectile total $C_{N_{\alpha_0}}$ is obtained by summing the wing and body contributions according to equation

$$C_{N_{\alpha 0}} = \left[C_{N_{\alpha 0}}\right]_b + K_{\text{int}_{wb}} K_{\text{int}_{ff}} \left[C_{N_{\alpha 0}}\right]_w \qquad 2\text{-}3$$

3. The projectile total lift force slope $C_{L_{\alpha_0}}$ is finally computed by subtracting the zero angle of attack drag C_{D_0} from normal force coefficient slope $C_{N_{\alpha_0}}$.

$$C_{L_{\alpha 0}} = C_{N_{\alpha 0}} - C_{D_0} \qquad 2\text{-}4$$

4. The detailed methods to determine the normal force coefficient slope components are presented in the **Annex E**.

2.3 MOMENT COMPUTATIONS

1. The pitch damping moment caused by fins is computed from equation

$$C_{m_q} + C_{m_\alpha} = -2 K_{\text{int}_{wb}} K_{\text{int}_{ff}} \left[C_{N_{\alpha 0}}\right]_w \left(\frac{\Delta x}{d}\right)^2 \qquad 2\text{-}5$$

2. The projectile total pitch damping moment coefficient is obtained by summing up the body and fin-set contributions.

3. The roll-producing moment coefficient is obtained from the equation

$$C_{l_0} = n_{fin} \frac{\left[C_{N_{\alpha 0}}\right]_w}{2} \delta_{eff} \frac{y_{arm}}{d} \qquad 2\text{-}6$$

4. The spin-damping moment coefficient $C_{l\hat{p}}$ is obtained from experimental-data-based relation

$$C_{l\hat{p}} = -2.15 \frac{C_{l_0}}{\delta_{eff}} \frac{y_{arm}}{d} \qquad 2\text{-}7$$

5. The Magnus moment (turning the nose left to negative direction if positive cant angle) is determined from

$$C_{n_\alpha} = -\left(\frac{8}{\pi}\right) K_{\text{int}_{wb}} K_{\text{int}_{ff}} \left[C_{N_{\alpha 0}}\right]_w \delta_{eff} \qquad 2\text{-}8$$

6. The detailed methods to determine the pitch damping moment, the roll-producing moment, the spin-damping moment coefficient and the Magnus moment are presented in the **Annex E**.

CHAPTER 3 GENERALISED YAW AERODYNAMICS

1. The effect of angle of attack α on aerodynamics is expressed in form

$$C_D = C_{D_0} + C_{D_{\alpha^2}} \alpha^2 \qquad 3\text{-}1$$

$$C_{L_\alpha} = C_{L_{\alpha 0}} + C_{L_{\alpha^3}} \alpha^2 \qquad 3\text{-}2$$

$$C_{m_\alpha} = C_{m_{\alpha 0}} + C_{m_{\alpha^3}} \alpha^2 \qquad 3\text{-}3$$

2. The subscript 0 is for the value at zero angle of attack. The effect of angle of attack will be taken into account only for the three coefficients presented in Equations 3-1 to 3-3 above.

3. The detailed methods to determine the coefficients above are presented in the **Annex F.**

INTENTIONALLY BLANK

ANNEX A LIST OF REQUIREMENTS, LIST OF SYMBOLS, COORDINATE SYSTEM

A.1. LIST OF REQUIREMENTS

The following parameters are used in the equations of this document.

Parameter	Unit	Parameter	Unit
Total length of projectile	[mm]	Number of Nubs	[-]
Length of cylindrical part	[mm]	Nub leading edge distance from nose	[mm]
Length of nose	[mm]	Nub root chord	[mm]
Length of base cone/flare	[mm]	Max cross-sectional area of Nubs	[mm^2]
Length of tail boom	[mm]	Nub Area center % (root chord)	[%]
Diameter of projectile	[mm]	Fin area of 1 nub	[mm^2]
Mass center from nose-tip	[mm]	Deflection angle, posit. causes positive spin	[deg]
Long. projected area of projectile	[mm^2]	Groove pattern length	[mm]
Center of projected area from nose-tip	[mm]	Wetted area coefficient	[-]
Volume of projectile	[mm^3]	Number of fins	[-]
Center of volume from nose-tip	[mm]	Airfoil type	[-]
Diameter of nose-tip	[mm]	Average WEDGE fraction (0..1)	[-]
Length of nose-tip	[mm]	Apex from nose	[mm]
Radius ratio of nose tip	[-]	Total span of wing	[mm]
Radius ratio of nose (0=cone, 1=tangent ogive)	[-]	Leading edge sweep angle	[deg]
1=Rotating Band exists, 0=Rotating Band does not exist	[-]	Length of wing root chord	[mm]
Outer diameter of rotating band	[mm]	Length of wing tip chord	[mm]
Number of grooves	[-]		
Distances from nose (to groove mid point)	[mm]	Wing max thickness/average wing chord length	[-]
Diameter of body (w/o groove)	[mm]	Blunt leading edge thickness / average wing chord length	[-]
True diameter of body (at groove bottom)	[mm]	Blunt trailing edge thickness / average wing chord length	[-]
Width of grooves	[mm]	Basic cant angle	[deg]
Number of steps	[-]	Bevelling effect: total	
Distances from nose	[mm]	Bevelling effect: w/o leading edge	
Diameter before step	[mm]	Gap between fin and body	[mm]
Diameter after step	[mm]	Roll position: 0 --> + position, 1 --> x-roll position	[-]
Forward facing step slope angle 0...90	[deg]		
Flight altitude	[m]		
Boundary layer at nose part : 1=laminar, 0=turbulent	[-]		

A.2. LIST OF SYMBOLS

A	aspect ratio axial force	$\frac{b^2}{S}$
a	speed of sound	
b , $b_{\exp}$	wing span, exposed wing span (without body contribution)	
C_A	axial force coefficient	$\frac{A}{qS}$
$\bar{c}_{dc}$	cross flow drag coefficient	
C_D	drag coefficient	$\frac{D}{qS}$
C_{D_0}	zero angle of attack drag coefficient	
C_{D_b}	base drag coefficient	
$C_{D_{bt}}$	boat-tail drag coefficient	
C_{D_c}	cylindrical drag coefficient	
C_{D_g}	grooves drag coefficient	
C_{D_f}	friction drag coefficient	$C_f \frac{S_{wetted}}{S}$
$C_{D_{fin}}$	fin drag coefficient at zero angle of attack	
$C_{D_{FL}}$	boat-tail/flare drag coefficient	
C_{D_n}	nose drag coefficient	
$C_{D_{Nubs}}$	nubs drag coefficient	
C_{D_p}	pressure drag coefficient	
$C_{D_{pr}}$	protuberance drag coefficient	
$C_{D_{\alpha^2}}$	quadratic yaw angle drag coefficient (STANAG 4355)	
C_f	friction coefficient	
C_{f_L}	laminar friction coefficient	
C_{f_T}	turbulent friction coefficient	
C_L	lift force coefficient	$\frac{L}{qS}$

C_{L_α}	lift force coefficient slope	$\frac{\partial C_L}{\partial \alpha}$
$C_{L_{\alpha_0}}$	lift force coefficient slope at zero angle of attack	
$C_{L_{\alpha^3}}$	cubic lift force coefficient (STANAG 4355)	
C_l	rolling moment coefficient	$\frac{\mathcal{L}}{qSd}$
$C_{l_{\dot{p}}}$	spin damping moment coefficient	$\frac{\partial C_l}{\partial\left(pd/2V\right)}$
C_{l_0}	roll-producing moment coefficient	$C_{l_\delta}\,\delta$
C_{l_δ}	roll-producing moment coefficient slope	
C_m	pitching (overturning) moment coefficient	$\frac{\mathcal{M}}{qSd}$
C_{m_q}	pitch damping moment coefficient	$\frac{\partial C_m}{\partial\left(Qd/2V\right)}$
$C_{m_q}+C_{m_{\dot{\alpha}}}$	sum of pitch damping moment coefficients	
C_{m_α}	pitching (overturning) moment coefficient slope	$\frac{\partial C_m}{\partial \alpha}$
$C_{m_{\alpha_0}}$	pitching (overturning) moment coefficient slope at zero angle of attack	
$C_{m_{\dot{\alpha}}}$	pitch damping moment coefficient	$\frac{\partial C_m}{\partial\left(\dot{\alpha}d/2V\right)}$
$C_{m_{\alpha^3}}$	cubic pitching (overturning) moment coefficient (STANAG 4355)	
C_n	yawing moment coefficient	$\frac{\mathcal{N}}{qSd}$
C_{n_α}	yaw (Magnus) moment coefficient slope caused by nubs or fins	$\frac{\partial C_n}{\partial \alpha}$
$C_{n_{p\alpha}}$	Magnus moment coefficient slope	$\frac{\partial^2 C_n}{\partial\left(pd/2V\right)\partial\alpha}$
C_N	normal force coefficient	$\frac{N}{qS}$
C_{N_α}	normal force coefficient slope	$\frac{\partial C_N}{\partial \alpha}$

$C_{N_{\alpha_0}}$	normal force coefficient slope at zero angle of attack	
C_p	pressure coefficient	
C_Y	side force coefficient	$\frac{Y}{qS}$
$C_{Y_{p\alpha}}$	Magnus force coefficient slope	$\frac{\partial^2 C_Y}{\partial\left(pd/2V\right)\partial\alpha}$
C_{wetted}	surface area ratio	
C.G.	center of gravity	
c	chord	
$\bar{c}$, *MAC*	mean aerodynamic chord	
D	drag	
d	diameter, projectile body diameter, caliber of the projectile	
FNF	normal force loss factor (due to fin-body gaps)	
g	gap between fin and body	
K, k	interference effect factor, shape factor	
L	lift force	
L	rolling moment	
l	length	
l_{eff}	projectile effective length	
LND	proportion of nose length (l_n) to body diameter (d)	$\frac{l_n}{d}$
LBD	proportion of body length (l_b) to body diameter (d)	$\frac{l_b}{d}$
M	pitching moment, overturning moment, pitch	
Ma	Mach number	$\frac{V}{a}$
N	yawing moment	
N	normal force	
n	number of parts	
p	projectile spin rate	
$\hat{p}$	dimensionless spin rate	$\frac{pd}{2V}$
q	kinetic pressure	$\frac{1}{2}\rho V^2$
r	radius	
r_{loc}	local body radius	
Re	Reynolds number	

RR	radius ratio, proportion of tangential radius (r') to radius of true curvature (r)	*RR=r'/r*
S	reference area	$\pi d^2/4$
S_c	lateral projection area	
S_{wetted}	surface wetted area (without base)	
SHAPF	nose shape factor	
t	thickness	
V	velocity	
V_B	volume of projectile	
y_{arm}	fin moment arm	
Y	side force	
Λ , $\Lambda_{c/2}$	sweep angle, half chord sweep angle	
α	angle of attack, yaw angle, yaw	
β	compressibility parameter	$\sqrt{\lvert Ma^2-1\rvert}$
δ	nub incidence angle	
δ_{eff}	effective fin cant angle	
ε	base cone/flare/boat-tail angle (negative angle value = flare)	
ρ	air density	
ν	kinematic viscosity	
μ	Mach angle	$\arcsin\frac{1}{Ma}$
Δx	distance between the center of gravity and the fin aerodynamic center	
x_{ac}	aerodynamic center	
x_{cg}	center of gravity	
x_{cp}	center of pressure	
$x_{forcecenter}$	center of force	
x'_{cp}	center of pressure in diameters	

Subscripts

av	average	*LE*	leading edge
B , b	body, base	*n*	nose
bt	boat tail, base cone / flare	*r*	root
c	cylinder	*t*	tip
exp	exposed wing	*tb*	tail boom
ff	fin-fin	*TE*	trailing edge
fin	fin	W , w	wing
FL	flare	*wb*	wing-body

g	groove	*wetted*	wetted area
int, *inf*	interference	*o*	zero angle of attack

A.3. COORDINATE SYSTEM

1. The positive directions of aerodynamic forces and moments are given in the figure below.

2. The total angle of attack α is the angle between the projectile longitudinal symmetry axis x and the velocity vector V.

3. The positive direction of Drag force vector D is parallel to the velocity vector, but to the opposite direction and Lift force vector L is perpendicular to the Drag vector. D and L also define the positive directions of the corresponding coefficients used in this document (CD, and CL).

4. The positive direction of axial force coefficient CA is the direction of the negative x-axis and the positive direction of the normal force coefficient CN is the direction of the negative z-axis.

5. The positive directions of the aerodynamic moments, rolling moment L, pitching moment M and yawing moment N are defined according to the right-hand rule as depicted in the figure below.

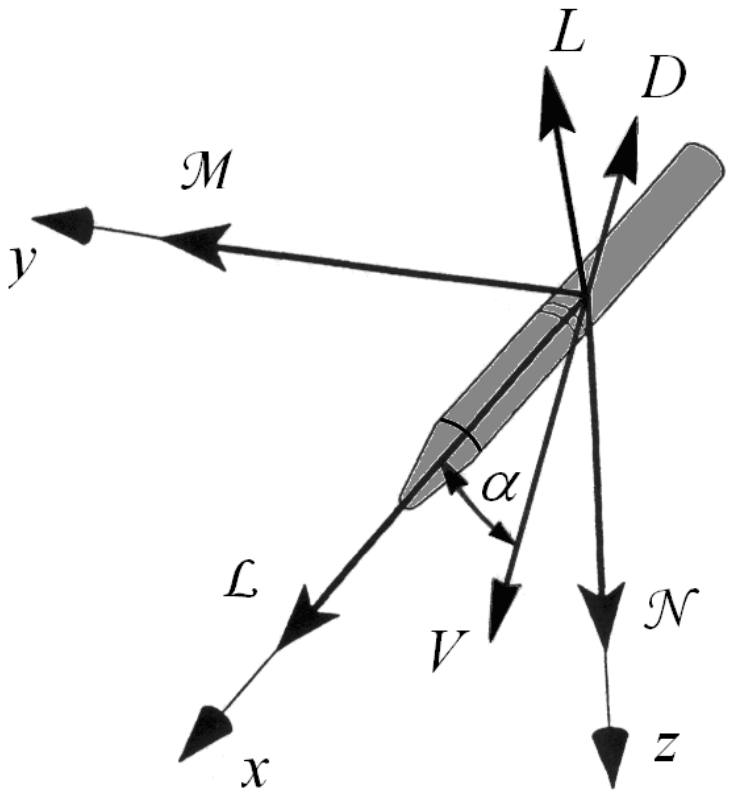
L
D
M
y
α
L
V
N
x
z

INTENTIONALLY BLANK

ANNEX B DRAG COMPUTATION METHODS FOR PROJECTILE BODY

1. The drag of a projectile can be divided into two parts: pressure drag and viscous (friction) drag. The former is typically calculated based on the engineering curves and the latter is calculated based on the measured values of equivalent flat-plate viscous drag. The complete zero angle of attack drag coefficient C_{D_0} is finally obtained by summing up the relevant, separately calculated pressure drag components and the viscous drag obtained for entire wetted area.

2. The zero angle of attack drag of a projectile consists of the pressure drag of the nose, flare, boat-tail, base (including possible tail boom), protuberances (driving band, grooves and steps), bourrelet nubs and of the viscous drag as a sum of the following form:

$$C_{D_0} = C_{D_n} + C_{D_{FL}} + C_{D_{bt}} + C_{D_b} + C_{D_{pr}} + C_{D_{Nubs}} + C_{D_f} \qquad \text{B-1}$$

3. The drag of the cylindrical part is entirely included to friction drag.

4. The drag coefficient is computed as a function of Mach number, also the effect of Reynolds number is taken into account via skin friction and base drag. The effect of angle of attack is taken into account through a corresponding coefficient used in a parabolic drag-approximation equation. The schematic of projectile geometry is depicted in Figure 1.

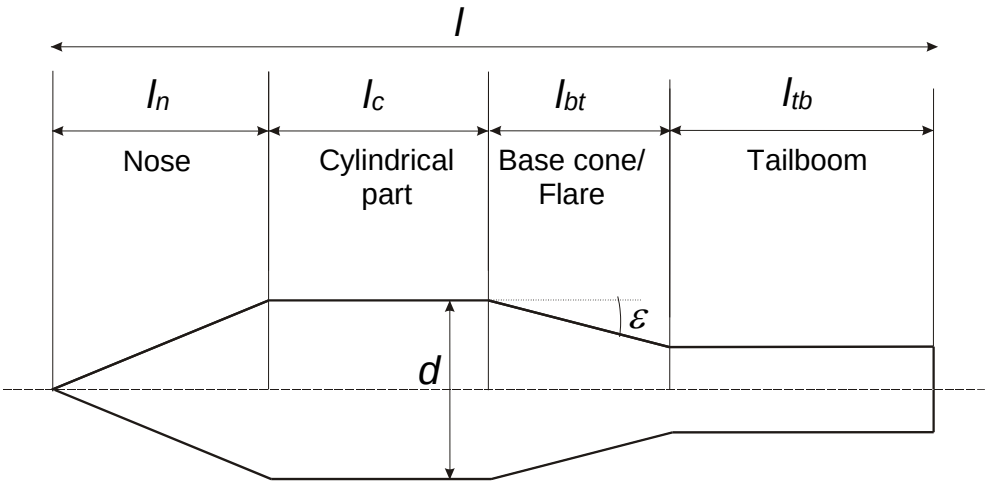

Figure 1: Schematics of projectile geometry. *l* is projectile length, l_n is length of nose, l_c is length of cylindrical part, l_{bt} is length of base cone/flare, l_{tb} is length of tailboom. Projectile diameter is *d* (reference diameter) and ε is base cone/flare angle (flare if angle negative).

B.1. NOSE AND FLARE PRESSURE DRAG

1. The nose pressure drag at **supersonic region** for a cone is calculated according to the equation B-2 giving the pressure coefficient on the nose surface. The second term takes into account the nose shape on drag (see Figure 2 and 3).

$$C_p = k_1 \sin^2 \varepsilon + k_2 \frac{\sin \varepsilon (\cos \varepsilon)^{Ma^{-RR}(16.5RR-2.5)\sin \varepsilon}}{Ma + \left[RR(1-RR)\right]^{0.5} \cos \varepsilon} \qquad Ma \geq 1 \qquad \text{B-2}$$

2. The coefficient k_1 is an average pressure coefficient on a blunt projectile face behind a normal shock wave and the coefficient k_2 takes into account the shape of the nose as a function of radius ratio parameter *RR*. These coefficients will be explained in detail later.

3. In case of a normal, slender projectile nose, the second term numerator is in practice $k_2 \sin \varepsilon$ and the equation can be written.

$$C_p = k_1 \sin^2 \varepsilon + k_2 \frac{\sin \varepsilon}{Ma + \left[RR(1-RR)\right]^{0.5} \cos \varepsilon} \qquad Ma \geq 1 \qquad \text{B-3}$$

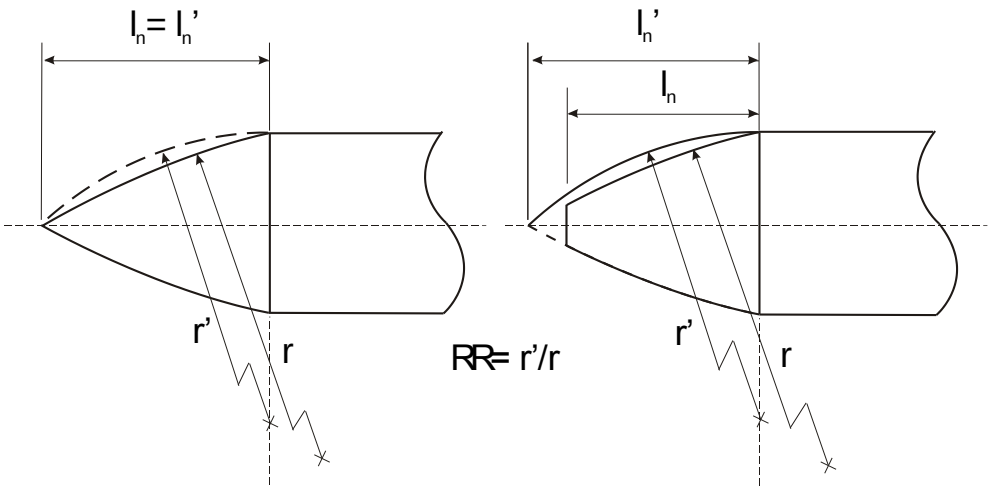

Figure 2: Variable *RR* (Radius Ratio) is defined as the proportion of tangential radius (r') to radius of true curvature (r). The radius r' is obtained from equation B-10. For non-sharp nose-tips, the tangential nose contour line is extended to the body centerline. The tangential radius is then computed using this nose length.

4. The equation B-2 is modified further into

$$C_p = k_1 \sin^3 \varepsilon_{av} + \frac{1}{2} \sin \varepsilon \cos^5 \varepsilon_{av} Ma^3 - (1 - Ma) \cos \varepsilon_{av} \qquad Ma < 2 \qquad \text{B-4}$$

5. The equation makes it possible to estimate the nose pressure drag at **subsonic** region for blunt noses. The average bluntness used at subsonic region (nose slope angle ε_{av}) is estimated from additional equation

$$\varepsilon_{av} = \sum \frac{\varepsilon_n}{\left(1 + \frac{RR_n}{4}\right)} \left[\left(\frac{d_n}{d}\right)^2 - \left(\frac{d_{n-1}}{d}\right)^2 \right] \qquad \text{B-5}$$

6. The pressure coefficient is taken to be 0 if the value given by equation B-4 is negative.

if $C_p < 0$ ➔ use $C_p = 0$ all speeds B-6

7. The coefficient k_1 is computed from B-7 and B-8, and the coefficient k_2 is computed according to B-9. The radius ratio *RR* in the equations is an inverse of the ratio of the true radius of curvature and the tangent-ogive radius *r'* (equation B-10). The nose contour line is to be extended to the projectile center line in case of blunted nose (see Figure 2). The extended nose length is used in equation B-10. The ratio *RR* is zero for a conical element.

$$k_1 = 1 - 0.2\sqrt{1 - Ma^2} \qquad 0 \le Ma < 1 \qquad \text{B-7}$$

$$k_1 = \frac{5}{3} - \frac{2}{3Ma^{\sqrt{2}}} \qquad 1 \le Ma \qquad \text{B-8}$$

$$k_2 = 0.9 - 0.9RR + RR^2 \qquad \text{B-9}$$

$$r' = \frac{l_n'^2}{d} + \frac{d}{4} \qquad \text{B-10}$$

$$RR = \frac{r'}{r} \qquad \text{B-11}$$

8. The equations presented here are used for all forward facing components (nose tip, nose and flare), and the cone half angle ε used in B-2 and B-4 is defined in Figure 3.

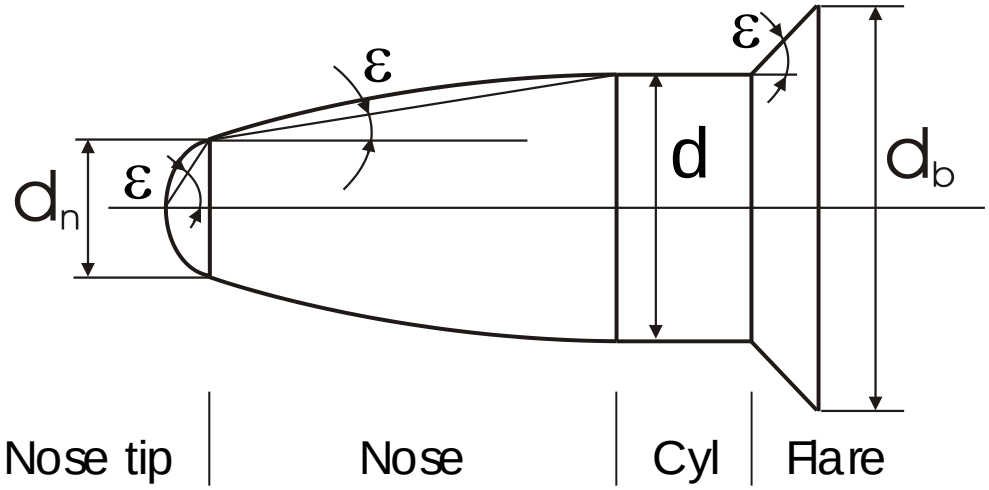

Figure 3: Cone half angle *ε* for forward facing surfaces. The value of *ε* is not affected by the component external form.

9. The nose pressure drag coefficient is computed as follows (n nose elements):

$$C_{D_{nose}} = \sum C_{p_n}\left[\left(\frac{d_n}{d}\right)^2 - \left(\frac{d_{n-1}}{d}\right)^2\right] \qquad \text{B-12}$$

10. The linear superposition method needs a modification for “convex” nose shapes; the term means here that the true body surface inclination angle increases while going downstream. The effective shape used for example for a blunt shoulder element is then the angle illustrated in Figure 4. The first order estimate for the subsonic/transonic effective angle is obtained by drawing a line from the mid-point of the previous element to the end-point of the current element (here the blunt shoulder). The effect of compressibility at the supersonic speed region is taken into account by dividing the angle value obtained by $Ma^{0.5}$, see equation B-13. We assume that this modest correction takes into account the larger drag reducing effect of spike at the high speeds. Nevertheless, the effective angle minimum is limited according to Figure 4; the limiting line is drawn from the leading edge of the previous element to the end-point of the latter one.

$$\varepsilon(Ma) = \frac{\varepsilon_{convexEffectivw}}{\sqrt{Ma}} \qquad \text{B-13}$$

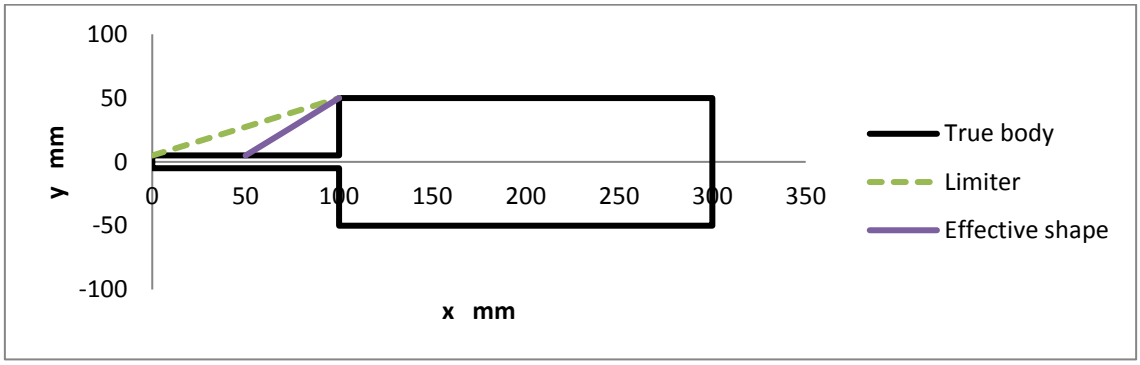

Figure 4: The effective nose shape when the inclination angle increases downstream. The effective angle is now applied for the blunt body part (at *x* = 100 mm) of the example shown.

10. The flare pressure drag is obtained from

$$C_{D_{FL}} = C_{p\,flare}\left[\left(\frac{d_b}{d}\right)^2 - 1\right] \qquad \text{B-14}$$

11. $C_{p_{nose}}$, $C_{p_{nose\text{-}tip}}$ and $C_{p_{flare}}$ are the pressure coefficients computed according to B-2 and B-4 for each projectile component.

12. The nose pressure drag computation method changes at some point when the speed increases from subsonic to transonic and supersonic region (Equations B-4 → B-2). The change is sudden and the smaller value obtained is applied at methods overlapping area. However, some averaging or smoothing method is needed there to make the behavior physically reasonable. At the overlapping region *Ma* = 0…2 the average of the current and previous nose pressure drag coefficient (f(*Ma*), obtained using B-13) values is used. The averaging relaxes the curve behavior without changing the result extensively if the drag computation Mach number is updated frequently enough particularly at the transonic speeds. The drag is obtained from an additional formula

$$C_{D_n}(i+1) = \frac{C_{D_n}(i+1) + C_{D_n}(i)}{2} \qquad \text{B-15}$$

13. The averaging “delays” a little bit of pressure drag rise but this is assumed not to deteriorate the method applicability/accuracy. This smoothing is carried out in order to avoid the pressure drag Mach trend abrupt when another method is taking over.

B.2 BOAT-TAIL PRESSURE DRAG

1. The boat-tail average pressure coefficient at **transonic and supersonic speeds** is computed from equation B-16. The term in the brackets takes into account the pressure recovery at the boat-tail surface.

$$C_p = -\frac{\sin \varepsilon_{bt}}{Ma}\left[1+\left(\frac{d_b}{d}\right)^2\right] \qquad Ma \geq 1.2 \qquad \text{B-16}$$

2. The boat-tail angle ε_{bt} is depicted in Figure 5.

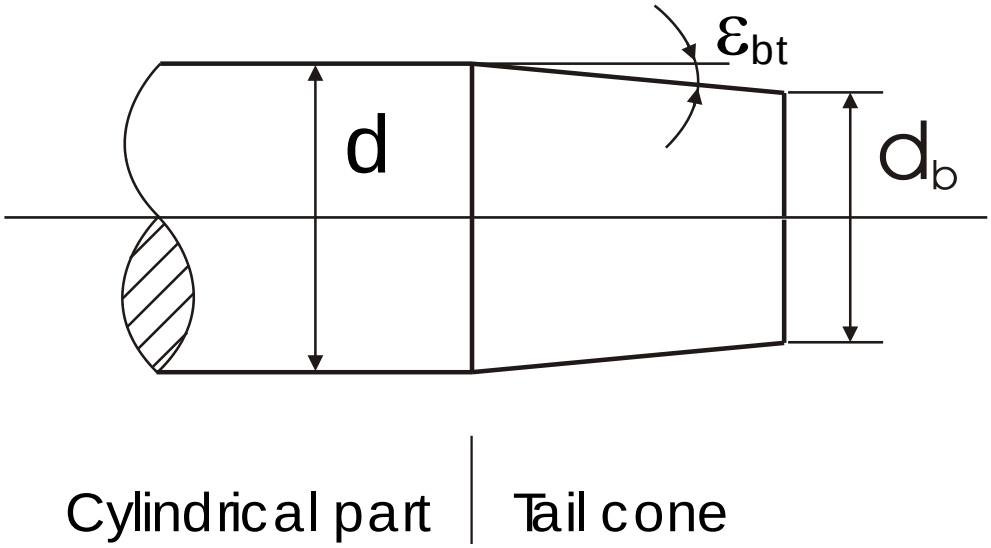

Figure 5: Boat-tail angle ε_{bt} and base diameter d_b.

3. The equation B-16 is further modified into B-17 to give drag estimate at **subsonic speed** particularly at large (unusual) ε_{bt}-angle values.

$$C_p = -\sin^3 \varepsilon_{bt}\left[1+\left(\frac{d_b}{d}\right)^2\right] \qquad 0.8 < Ma \qquad \text{B-17}$$

5. The boat-tail pressure drag coefficient $C_{D_{pbt}}$ is computed from equation

$$C_{D_{p_{bt}}} = -C_p\left[1-\left(\frac{d_b}{d}\right)^2\right] \qquad \text{B-18}$$

6. The projectile boat-tail drag is obtained from a fit at transonic region. The limits of transonic region are defined to be 0.8 and 1.2.

7. The fitted boat-tail drag is calculated from equation

$$C_D(Ma) = \frac{C_{D_{1.2}} - C_{D_{0.8}}}{(1 + e^{-20(1-Ma)})} + C_{D_{0.8}} \qquad \text{B-19}$$

8. The total subsonic base area drag (the boat-tail and the blunt base) will reach the blunt base drag at about ε_{bt}-angle 30 degree when equation B-18 and the subsequent base-drag equations (B-32) are used. Above that, the flow is assumed to be completely separated, and the base area drag is limited up to the blunt base value.

9. The boat-tail drag is obtained from equation

$$C_{D_{pbt}} = C_{D_{bc}} - C_{D_b} \qquad \text{B-20}$$

B.3 BASE PRESSURE DRAG

B.3.1 An infinite long cylinder

1. The pressure coefficient on the base of a long cylinder is computed at **subsonic** speeds (up to Mach 0.8) from

$$C_{p_{bc}} = \frac{-0.029}{\sqrt{C_{D_{forebody}}}} \qquad Ma \leq 0.8 \qquad \text{B-21}$$

2. The term $C_{D_{forebody}}$ (forebody drag coefficient) includes the viscous and the rotating band drag.

3. At **supersonic** velocities (1.2 < *Ma*), the coefficient is computed from

$$C_{p_{bc}} = -0.31e^{-0.37Ma} \qquad Ma > 1.2 \qquad \text{B-22}$$

4. The projectile base drag is obtained from a fit at transonic region. The limits of transonic region are defined to be 0.8 and 1.2.

5. The fitted projectile base drag is calculated from equation

$$C_D(Ma) = \frac{C_{D_{1.2}} - C_{D_{0.8}}}{(1 + e^{-20(1-Ma)})} + C_{D_{0.8}} \qquad \text{B-23}$$

6. The Reynolds number is assumed to have no effect on the base pressure at supersonic speeds.

B.3.2 A finite long cylinder

The base pressure coefficient value for an infinite cylinder is further modified to take into account the effect of cylinder finite length and the nose when Ma < 3. The interpolation between the cylinder and the disc values is presented in the context of a **flare base** projectile, for which the base drag is computed according to Equation B-29. The ε –value used for a non-flare base projectile is the one for the nose.

B.3.3 A flare base

1. In case of a **flare** base projectile, the base pressure coefficient C_{p_b} is interpolated (equation B-27) between the coefficient values behind an infinitely long cylinder and a disc as a function of flare angle ε (Figure 3). The coefficient value for the infinite long cylinder is computed according to equations B-21 and B-22, and the value behind the disc is estimated via equations B-24, B-25 and B-26.

$$C_{p_{b_{disc}}} = -0.5 \qquad 0 < Ma \leq 1.41 \qquad \text{B-24}$$

$$C_{p_{b_{disc}}} = -\frac{1}{Ma^2} \qquad 1.41 < Ma \leq 3 \qquad \text{B-25}$$

$$C_{p_{b_{disc}}} = C_{p_{bc}} \qquad 3 < Ma \qquad \text{B-26}$$

$$C_{p_{b_{FL}}} = -\left|\left(\left|C_{p_{b_{disc}}}\right| - \left|C_{p_{b_c}}\right|\right)\sqrt{\sin\varepsilon} + \left|C_{p_{b_c}}\right|\right| \qquad \text{B-27}$$

$C_{p_{bc}}$ is obtained according to B-21 and B-22.

2. The flare base value given by equation B-27 is modified to take into account the cylinder length behind the flare (or nose). This is achieved by taking into account the cylinder length via interpolation:

$$C_{p_b} = -\left|C_{p_{b_{FL}}} - \left(\left|C_{p_{b_{FL}}}\right| - \left|C_{p_{b_c}}\right|\right)\sqrt[3]{\frac{l}{3d}}\right| \qquad l < 3d \qquad \text{B-28}$$

where

l = length of the following cylinder
d = diameter of the following cylinder

3. The flare/nose effect is assumed to vanish during the length of 3 local diameters (cylindrical body or tail boom).

4. The base drag coefficient for a flare base projectile is computed from equation

$$C_{D_b} = -C_{p_b}\left(\frac{d_b}{d}\right)^2 \qquad \text{B-29}$$

B.3.4 A boat-tailed base

1. In the case of a **boat-tailed** base (see Figure 5), the pressure coefficient C_{p_b} is computed as

$$C_{p_b} = \left(\frac{d_b}{d}\right)^x C_{p_{b_c}} \qquad \text{B-30}$$

2. The pressure coefficient $C_{p_{b_c}}$ in the equation is the one valid for **a finite length** cylinder base (see the **flare base** projectile equation B-28).

3. The exponent *x* is taken to be 2 at subsonic speeds (*Ma* < 0.8) and 1 at supersonic region (*Ma* > 1.2). At transonic region (0.8 ≤ *Ma* ≤ 1.2) the exponent is obtained from equation B-31.

$$x(Ma) = -\frac{1}{(1+e^{-20(1-Ma)})} + 2 \qquad \text{B-31}$$

3. The tail-boom length effect on the base pressure coefficient is taken into account like in case of a flare base projectile.

4. The base drag coefficient C_{D_b} is computed from equation B-32

$$C_{D_b} = -C_{p_b}\left(\frac{d_b}{d}\right)^2 \qquad \text{B-32}$$

5. The projectile base area total drag is limited up to the blunt base (cylinder) value (according to B-29) in case the base and boat-tail drag sum ($C_{D_{pbt}} + C_{D_b}$) exceeds the blunt base value. The boat-tail pressure drag is limited in case according to equation B-20.

B.4 FRICTION DRAG AND SPIN DAMPING

B.4.1 Skin friction drag

1. Skin **friction drag** is calculated by equation

$$C_{D_f} = C_f \frac{S_{wetted}}{S} \qquad \text{B-33}$$

where

C_f = mean friction coefficient (B-34 or B-35) for a smooth flat plate

S_{wetted} = computed wetted surface area

S = reference area $= \frac{\pi d^2}{4}$

C_{D_f} = friction drag coefficient

2. The turbulent boundary-layer friction coefficient C_{f_T} is computed by equation

$$C_{f_T} = \frac{0.455}{(\log \mathrm{Re}_l)^{2.58}} \left(1 + 0.21 Ma^2\right)^{-0.32} \qquad \text{B-34}$$

where

C_{f_T} = turbulent friction coefficient

Re_l = Reynolds number $= \frac{Vl}{\nu}$

l = projectile/nose length

ν = kinematic viscosity

3. The laminar boundary-layer friction coefficient C_{f_L} is computed by equation

$$C_{f_L} = \frac{1.328}{\sqrt{\mathrm{Re}_l}} \left(1 + 0.12 Ma^2\right)^{-0.12} \qquad \text{B-35}$$

4. The boundary layer can be calculated as completely turbulent or assuming the nose boundary layer to be laminar.

5. The kinematic viscosity ν is computed from

$$\nu = \frac{\mu}{\rho} \qquad \text{B-36}$$

6. The air density ρ is computed according to ICAO standard atmosphere.

7. The dynamic viscosity μ is obtained from the Sutherland equation

$$\mu = \frac{C_1 T^{1.5}}{T + C_2} \qquad \text{B-37}$$

where

$C_1 = 1.458\text{e}^{-6} \dfrac{\text{kg}}{\text{ms}\sqrt{\text{K}}}$

C_2 = 110.4 K

T = air temperature, obtained from ICAO atmosphere model.

B.4.2 Spin damping coefficient

The **spin damping coefficient** C_{l_p} caused by friction is given by

$$C_{l_p} = -\frac{1}{2} C_{D_f} \qquad \text{B-38}$$

where

C_{l_p} = spin damping coefficient

C_{D_f} = friction drag coefficient

B.5 PROTUBERANCE DRAG

B.5.1 Forward/backward facing steps and the rotating band

1. The protuberance drag (like that of a rotating band) is computed by estimating the forward and backward facing surface pressure drag separately. The forward facing surface pressure coefficient is estimated according to B-40 or B-42 and the backward facing surface pressure coefficient is estimated according to B-39 or B-41.

2. The equations for the step pressure coefficients at subsonic velocities are

$$C_{p_{StepBW}} = -0.3 \qquad Ma < 1 \text{ (backward)} \qquad \text{B-39}$$

$$C_{p_{StepFW}} = 0.4 \sin \varepsilon \qquad Ma < 1 \text{ (forward)} \qquad \text{B-40}$$

3. The equations for the step pressure coefficients at velocities above speed of sound are

$$C_{p_{StepBW}} = -0.65 Ma^{-1.68} \qquad Ma \geq 1 \text{ (backward)} \qquad \text{B-41}$$

$$C_{p_{StepFW}} = (-0.067(Ma - 1) + 0.4) \sin \varepsilon \qquad Ma \geq 1 \text{ (forward)} \qquad \text{B-42}$$

4. The pressure coefficient values change linearly from zero to estimated values between the step-height values (h_{step}/d_{local}) 0 and 0.05.

$$C_p = 20\frac{h_{step}}{d_{local}}C_{p_{computed}} \qquad \text{if } \frac{h_{step}}{d_{local}} < 0.05 \qquad \text{B-43}$$

5. A step-like protuberance drag is obtained by

$$C_{D_{step}} = \left|C_p\right|\frac{S_{forehead}}{S} \qquad \text{B-44}$$

6. The rotating band drag is taken as a sum of forward and backward facing steps and is assumed to be valid for a launched band geometry without any spin effects.

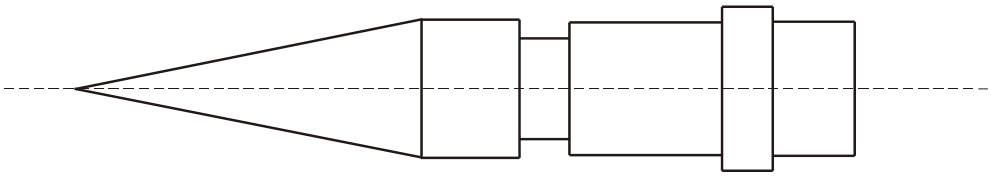

Figure 6: A schematic projectile geometry with a groove and a rotating band.

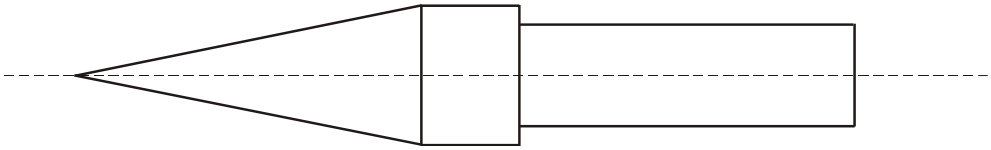

Figure 7: A schematic projectile geometry with a backward facing step

B.5.2 Transverse grooves

1. The drag caused by shallow transverse grooves is computed in a similar way as the individual step drag. The pressure coefficient sum (of the backward and forward facing parts) will change linearly between the sum and 0 when the ratio e/h (width/depth of groove) goes from 7 to 0.

$$C_{D_{groove}} = \frac{e}{7h}C_{D\,grooveComputed} \qquad \text{if } \frac{e}{h} < 7 \qquad \text{B-45}$$

2. Above the value of seven, the sum is used at it is obtained. This simplified method to take into account the interaction between the steps is used here at all speeds.

B.5.3 Groove pattern

1. Certain types of finned projectiles have a relatively large groove pattern on the surface of the cylindrical part of body. These grooves are needed at the internal ballistic phase and after launch, the grooves cause an unfavorable flow retarding effect.

2. The drag of excessive amount of grooves (see Figure 8) is computed from equation

$$\Delta C_{D_g} = 1.6 \frac{l_g}{l_c} C_{SFSB} (C_{wetted} - 1) \qquad \text{B-46}$$

3. The coefficient C_{SFSB} is the viscous drag coefficient (equation B-33) of body cylinder part and the coefficient C_{wetted} is used to take into account the groove depth on drag. The coefficient is the surface area ratio of grooved cylinder length to that of same length cylinder without grooves; the incremental drag will be zero in case the surface coefficient C_{wetted} is 1.

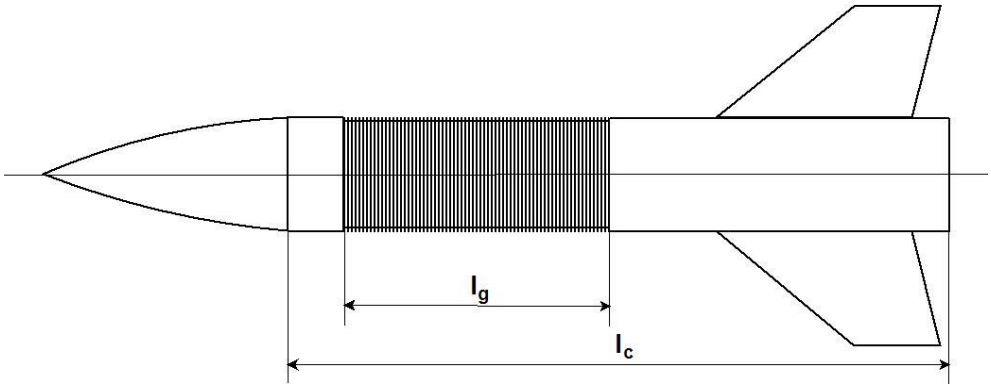

Figure 8: Groove pattern area on the surface of the cylindrical part of body. Length of grooved area (l_g) and length of cylindrical body (l_c).

B.5.4 Total protuberance drag

The total protuberance drag is obtained from equation

$$C_{D_{pr}} = \sum C_{D_{step}} + C_{D_{rotatingband}} + \sum C_{D_{groove}} + \Delta C_{D_g} \qquad \text{B-47}$$

B.6 BOURRELET NUBS

1. The zero angle of attack drag caused by bourrelet nubs is computed by scaling the drag of one nub as a linear function of its squared fineness ratio. The drag coefficient for **one** nub is 0.0025 (ref. area S = πd^2/4) and this result is obtained when the squared fineness ratio is 100. The ratio is computed by

$$finenessratiosquared = \frac{c^2_{root}}{A_{\max\ frontal}} \quad \text{B-48}$$

2. The drag of one nub is obtained from

$$C_{D_{nub}} = 0.0025 \frac{100}{finenessratiosquared} \quad \text{B-49}$$

3. The nub chord c and the maximum frontal area of a nub are depicted in Figures 9 and 10. The nub cant angle δ (Figure 9) effect on the drag is proposed to be taken into account by using the root chord value (in the case of a non-spinning projectile).

$$c_{root} = c \cos \delta \quad \text{B-50}$$

4. The nub cant angle needs to be limited to some value less than 90°.

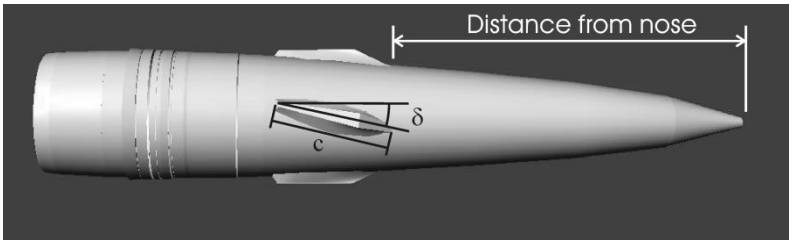

Figure 9: Nub root chord and cant angle.

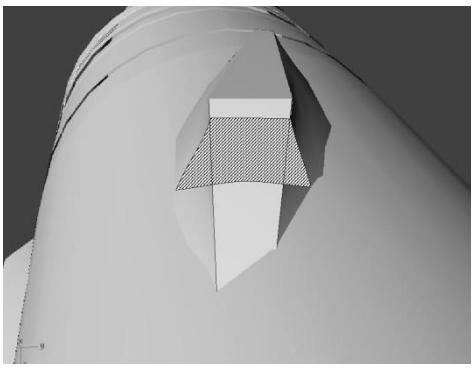

Figure 10: Nub max frontal area.

ANNEX C LIFT FORCE AND MOMENT COMPUTATION METHODS FOR PROJECTILE BODY

C.1 LIFT FORCE COMPUTATION

1. The zero lift force slope estimated in this chapter is valid at zero angle of attack. A projectile geometry with the nomenclature used is depicted in Figure 1.

2. The zero lift force coefficient slope is derived from computed normal force coefficient slope and zero angle of attack drag

$$C_{L_{\alpha_0}} = C_{N_{\alpha_0}} - C_{D_0} \qquad \text{C-1}$$

3. The normal force coefficient slope is obtained as a sum of the component slopes

$$C_{N_{\alpha 0}} = C_{N_{\alpha_{n_0}}} + C_{N_{\alpha_{b_0}}} + \Delta C_{N_{\alpha 0}} \qquad \text{C-2}$$

C.2 LIFT FORCE

The aerodynamics at supersonic region are computed based on hypersonic similarity parameters. The closed-form equations presented here provide a simple way to estimate the aerodynamics based on sound physical parameters.

The radius ratio *RR* is now at this context replaced by a nose cross-section area ratio parameter (see Figure 11 and Equation C-4). This is due to the more complex nose geometries to be handled. The term A_{cr} is the true nose cross section area and the A_{cone_cr} is the area of cone of the same length; the cross-section areas are shown in Figure 11. The equation presented is now a first order approximation for nose shape expressed earlier by the radii data (*RR*). The novel nose total *RR* -value may be obtained from the connection C-4.

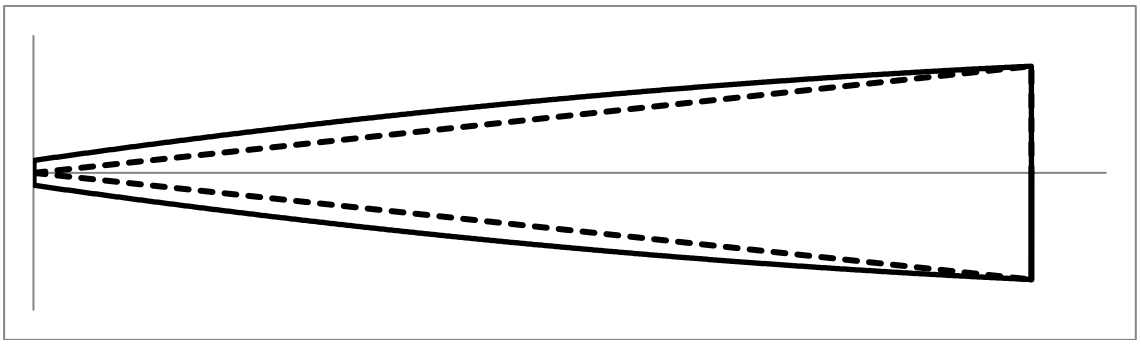

Figure 11: An example of some true nose geometry (with solid line) and a cone of the same length and body junction diameter.

C.2.1 Nose normal force coefficient slope

1. At **supersonic speeds** (when $Ma \geq 1.2$) the nose normal force coefficient slope is computed from

$$C_{N_{\alpha_{n0}}} = 2 * LF\left[SHAPF1 + RR\left(1 - \frac{\beta}{LND}\right)\frac{\beta}{LND}\right] \qquad \frac{\beta}{LND} < 1 \qquad \text{C-3}$$

$$SHAPF1 = 1 + \frac{RR}{10} = \left(\frac{A_{cr}}{A_{cone\_cr}}\right)^{0.25} \qquad \text{(nose shape factor 1)} \qquad \text{C-4}$$

or

$$C_{N_{\alpha_{n0}}} = 2 * LF\left[SHAPF2 + \frac{RR}{10}\left(1 - \left(\frac{\beta}{LND}\right)^{0.5}\right)\right] \qquad \frac{\beta}{LND} \geq 1 \qquad \text{C-5}$$

$$SHAPF2 = 1 + \frac{RR}{10} + \left(\frac{RR-1}{10}\right)\left(1 - \frac{LND}{\beta}\right)^{0.5} \qquad \text{(nose shape factor 2)} \qquad \text{C-6}$$

where

β = $\sqrt{Ma^2 - 1}$

RR = radius ratio (nose). See Figure 11 and Equation C-4.

$$LND = \frac{l_n}{d} \qquad \text{C-7}$$

where

l_n = nose length

d = body diameter

2. The length factor LF takes into account the finite nose length effect on the slope and will get values

LF = 1 if LND >1 C-8

LF = LND if LND ≤1 C-9

3. The nose normal force coefficient is computed for a cone-like shape if the true nose cross-section area is **smaller** than the conical area (*RR* < 0); for the smaller cross-section area noses the slope is estimated simply as scaled based on the cross-section area ratio

$$C_{N\alpha} = C_{N\alpha\_cone}\left(\frac{A_{cr}}{A_{cone\_cr}}\right)^2 \qquad \text{C-10}$$

3. At **subsonic and transonic speeds** (when 0< *Ma* <1.2) the nose normal force coefficient slope is computed according to the equation below

$$C_{N_{\alpha_{n_0}}} = \left(0.77 + 0.23Ma^2\right)C_{N_{\alpha_{n_{Ma=1.2}}}} \qquad 0 < Ma < 1.2 \qquad \text{C-11}$$

where

$C_{N_{\alpha_{n_{Ma=1.2}}}}$ = $C_{N_{\alpha_n}}$ at speed Ma 1.2

C.2.2 Body normal force coefficient slope

1. At **supersonic speeds** (when $Ma \geq 1.2$) the body (behind the nose) normal force coefficient slope is obtained using equations

$$C_{N_{\alpha_{b_0}}} = \frac{2LF}{SHAPF3}\left(\frac{LBD}{LBD + LND}\right)\left(\frac{\beta}{LND}\right)^{0.5(1+RR))} \qquad \frac{\beta}{LND} < 1 \qquad \text{C-12}$$

$$SHAPF3 = 1 + \frac{RR}{10} \qquad \text{(nose shape factor 3)} \qquad \text{C-13}$$

or

$$C_{N_{\alpha_{b_0}}} = \frac{2LF}{SHAPF3}\left(\frac{LBD}{LBD + LND}\right)\left(\frac{\beta}{LND}\right)^{-0.5RR} \qquad \frac{\beta}{LND} \geq 1 \qquad \text{C-14}$$

$$LBD = \frac{l_b}{d} \qquad \text{C-15}$$

$$l_b = l_c + l_{bt}\left(\frac{d_b}{d}\right)^2 \qquad \text{C-16}$$

where

d = body diameter

l_c = cylindrical part length

l_{bt} = boat-tail length

d_b = body base diameter

2. The value of LBD is limited to 3.

4. The method still includes almost the entire boat-tail length to the body carry-over length in case boat-tailing is negligible. On the other hand with the new formula the carry-over length and lift are not exaggerated particularly in case of long and steep mortar-shell boat-tails. The entire boat-tail l_{bt} and the tail-boom l_t lengths are included to the carry-over value in case the given boat-tail angle is zero degrees and some non-zero l_{bt} is given as input (up to the limiting dimensionless value 3).

2. The short body length (l_b) and the effect of Mach number are taken into taken account like in the equations for nose (C-3 to C-11) (substitute LND $\rightarrow$ LBD). The length factor LF takes into account the finite nose length effect on the slope and will get values

LF = 1 if LBD>1 C-17

$LF = LBD$ if $LBD \leq 1$ C-18

3. At **subsonic and transonic speeds** (when 0 < *Ma* < 1.2) the body normal force coefficient slope is computed according to equation

$$C_{N_{\alpha_{b_0}}} = \left(0.77 + 0.23Ma^2\right) C_{N_{\alpha_{b_{Ma=1.2}}}} \qquad \left(0 < Ma < 1.2\right) \qquad \text{C-19}$$

where

$C_{N_{\alpha_{b_{Ma=1.2}}}}$ = $C_{N_{\alpha_b}}$ at speed Ma 1.2

4. The interference effect from nose to boat-tail is taken into account by replacing the body length by the sum of the body and boat-tail lengths if the former dimensionless value is smaller than 3 ("semi-infinite length" here). However, the maximum value used for the sum is 3. This body length is used also when computing the body center of pressure.

5. The boat-tail lift-decreasing effect will be taken into account in the chapter C.3.

C.3 BOAT-TAIL, FLARE AND TAILBOOM LIFT FORCE

1. The change of normal force coefficient due to the **boat-tail** (see Figure 12) is computed using equations

$$\Delta C_{N_{\alpha 0}} = -2\left(0.77 + 0.23Ma^2\right)\cos^x \varepsilon_{bt}\left[1-\left(\frac{d_b}{d}\right)^2\right] \qquad Ma<1 \qquad \text{C-20}$$

$$\Delta C_{N_\alpha} = \frac{-2\cos^x \varepsilon_{bt}}{Ma^x}\left[1-\left(\frac{d_b}{d}\right)^2\right] \qquad Ma\geq 1 \qquad \text{C-21}$$

2. The tailboom effect is neglected for projectiles with boat-tail geometry.

$$x = \frac{d}{l_{bt}} \qquad \text{when } \frac{d}{l_{bt}}<1 \qquad \text{C-22}$$

$$x = 1 \qquad \text{when } \frac{d}{l_{bt}}\geq 1 \qquad \text{C-23}$$

3. The *Ma*-term in the equations takes into account the compressibility. The effect of boat-tailing will get smaller with growing boat-tail angle according to the cosine-term.

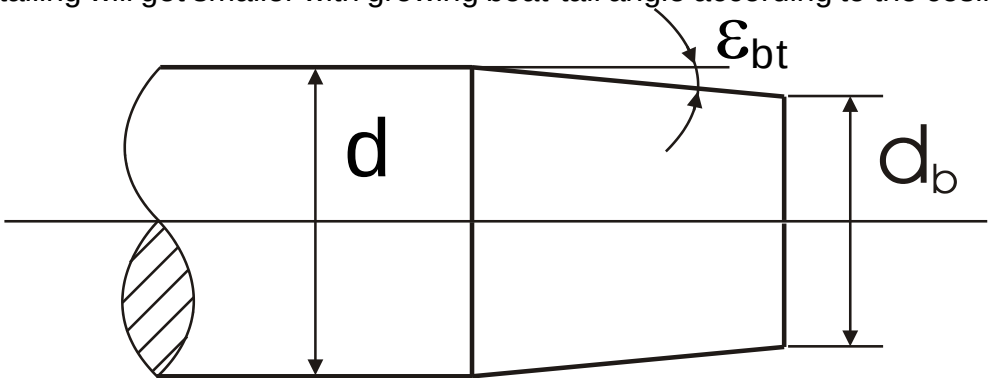

Figure 12: A boat-tailed projectile base geometry.

4. The increment of normal force coefficient due to the **flare** and possible tailboom is

$$\Delta C_{N_\alpha} = 2*(0.9)\cos^2 \varepsilon_{eff}\left[\left(\frac{d_b}{d}\right)^2 - 1\right] \qquad \text{C-24}$$

5. The flare-angle ε_{eff} is the true angle ε in case no tailboom is present (see Figure 13). The use of effective angle takes into account some of the lift carry-over to the tailboom.

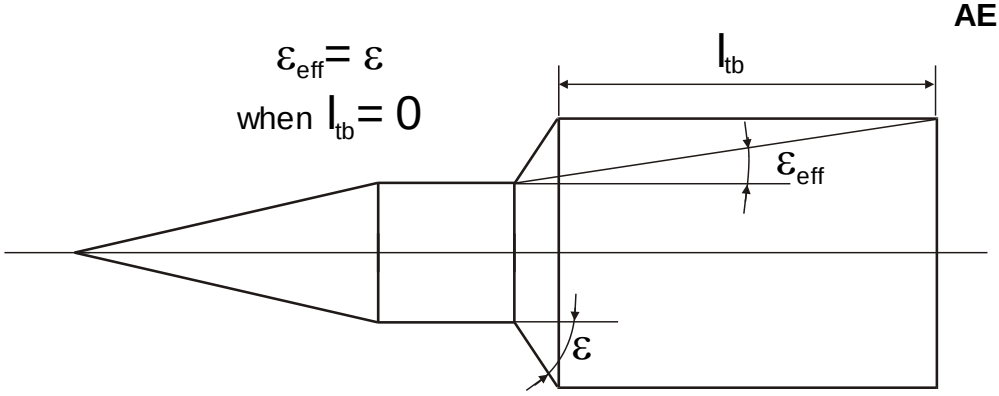

Figure 13: Flare-base projectile geometry.

C.4 MOMENT COMPUTATION METHODS

The moment coefficient slopes estimated in this chapter are computed as a function of Mach number and are valid at zero angle of attack. The effect of a high angle of attack is taken into account in Annex F. The zero pitching moment coefficient slope is obtained as a sum of the component slopes

$$C_{m_{\alpha 0}} = C_{m_{\alpha_{n0}}} + C_{m_{\alpha_{b0}}} + \Delta C_{m_{\alpha 0}} \qquad \text{C-25}$$

C.5 PITCHING MOMENT

1. The **nose** force center is taken to be cross area center (x_{cp_n} , measured from the nose tip)

$$x_{cp_n} = x_{noseCrossAreaCenter} \qquad \text{C-26}$$

2. The **body** (behind the nose) center of pressure (when Ma ≥ 1.2) is computed from

$$x_{cp_b} = \frac{LBD * LND}{LBD^2 + LND^2} * k_a \qquad \text{C-27}$$

$$k_a = \frac{\beta}{LND} \quad \text{when} \quad \frac{\beta}{LND} < \frac{LBD}{LND} \qquad \text{C-28}$$

$$k_a = \frac{LBD}{LND} \quad \text{when} \quad \frac{\beta}{LND} \geq \frac{LBD}{LND} \qquad \text{C-29}$$

3. The dimensionless value as body diameters (backwards from the nose-body junction) is computed from

$$x'_{cp_b} = LBD * x_{cp_b} \qquad \text{C-30}$$

4. The center of pressure location obtained at *Ma* 1.2 is also used in subsonic and transonic regions.

5. The contributions of **nose** and **body** to the pitching moment coefficient slope are computed as follows:

$$C_{m_{\alpha_n}} = \left(\frac{x_{cg} - x_{cp_n}}{d} \right) C_{N_{\alpha_n}} \qquad \text{C-31}$$

$$C_{m_{\alpha_b}} = \left[\frac{x_{cg}}{d} - \left(LND + x'_{cp_b} \right) \right] C_{N_{\alpha_b}} \qquad \text{C-32}$$

C.6 BOAT-TAIL, FLARE AND TAILBOOM PITCHING MOMENT

1. The change of the pitching moment coefficient slope due to the boat-tail or the flare and tailboom are

$$\Delta C_{m_\alpha} = \Delta C_{N_\alpha} \left(\frac{x_{cg} - \left(l_n + l_b + 0.5 l_{bt} \right)}{d} \right) \qquad \text{boat-tail} \qquad \text{C-33}$$

$$\Delta C_{m_\alpha} = \Delta C_{N_\alpha} \left(\frac{x_{cg} - \left(l_n + l_b + 0.6 l_{fl} + l_{tb} \sin \left| \varepsilon_{eff} \right| \right)}{d} \right) \qquad \text{flare} \qquad \text{C-34}$$

2. The force is assumed to affect at a point 50% of the boat-tail length (first order approximation) and at 60% station (backwards from the junction) in case of flare base

Boat-tail force center $x_{cp_{bt}} = 0.5 l_{bt}$ (backwards from the junction) C-35

Flare force center $x_{cp_{fl}} = 0.6 l_{fl}$ (backwards from the junction) C-36

3. The tailboom effect is neglected in equation C-33. The sin-term takes into account some of the carry-over effect in case of a flare+tailboom base; however, the aerodynamics is assumed to be dominated by fins present at tailboom.

C.7 PITCH DAMPING MOMENT

1. The sum of pitch damping moment coefficients is computed from

$$C_{m_q} + C_{m_\alpha} = -2 C_{N_\alpha} \left(\frac{l}{d} \right)^2 \left(l_{eff} - \frac{x_{cg}}{l} \right)^2 \qquad \text{C-37}$$

2. The projectile effective length l_{eff} is here

$$l_{eff} = \sqrt{0.77 + 0.23 Ma^2} \qquad 0 < Ma \leq 1.2 \qquad \text{C-38}$$

$$l_{eff} = \sqrt{0.77 + 0.23 * 1.2^2} \qquad 1.2 < Ma \qquad \text{C-39}$$

C.8 MAGNUS FORCE AND MOMENT

1. The Magnus force coefficient slope $C_{Y_{p\alpha}}$ is calculated by

$$C_{Y_{p\alpha}} = k(Ma)\frac{V_B}{5d_b^3} \qquad \text{C-40}$$

where

$k(Ma)$ = coefficient taking into account the Mach number
V_B = body volume
d_b = base diameter

The reference value 5 is the $\frac{V_B}{d_b^3}$ value of a typical projectile geometry .

2. The equation gives a large Magnus force if projectile is long and particularly if the base is boat-tailed.

3. The coefficient $k(Ma)$ value is taken to be constant 1 when $Ma \geq 2$. It's value changes here linearly from 0.5 to 1 when Mach-number grows from 0 to 2 to make the general behavior of the coefficient resemble the typical results in literature. It is also taken to be 1 when *Ma* is between 0.95 and 1 to somehow model the transonic peak. The coefficient $k(Ma)$ value varies linearly from value –2.0 (*Ma* = 0) to value 1.0 (*Ma* = 2) in case of a small-caliber projectile.

$$k(Ma) = \frac{Ma}{4} + 0.5 \qquad 0 \leq Ma < 0.95 \qquad \text{C-41}$$

$$k(Ma) = 1 \qquad 0.95 \leq Ma < 1 \qquad \text{C-42}$$

$$k(Ma) = \frac{Ma}{4} + 0.5 \qquad 1 \leq Ma < 2 \qquad \text{C-43}$$

$$k(Ma) = 1 \qquad 2 \leq Ma \qquad \text{C-44}$$

$$k(Ma) = \frac{3}{2}Ma - 2 \qquad \text{(small-caliber)} \qquad 0 \leq Ma \leq 2 \qquad \text{C-45}$$

4. The Magnus force typically affects at the rear part of projectile, where the boundary layer is thicker (here at the point 80 % of projectile length measured from nose tip). In case of boat-tailed projectile, force center at transonic region is taken to

be at $l_{bt}\sqrt{1-\frac{d_b}{d}}$ backwards from the starting point of the cone. This is needed to explain, typically fairly large, moment peak at this region. The behavior might be caused by the shock-wave/boundary layer interaction.

5. The Magnus moment coefficient slope is computed from

$$C_{n_{p\alpha}} = C_{Y_{p\alpha}} \frac{\left(x_{cg} - x_{forcecenter}\right)}{d} \qquad \text{C-46}$$

6. A coefficient value $k(Ma)=1$ may be used when creating input data for simplified trajectory models not including the corresponding moment.

7. The Magnus phenomenon (moment coefficient C_{n_α}) caused by the nubs is computed according to Eq. C-51.

C.9 BOURRELET NUBS

All the coefficients calculated here are summed up with the corresponding coefficients of projectile body. See Equations C-1, C-25, C-46, E-19, B-38 and E-22.

C.9.1 Lift force

1. The lift force coefficient slope for a **pair of nubs** is computed here from

$$C_{L\alpha_{nubpair}} = \frac{\pi A_{\exp}}{2}\left(1+\frac{d}{b}\right)^2 \frac{S_{\exp}}{S} \qquad \text{C-47}$$

where

$A_{\exp}$ = exposed aspect ratio
(without the body contribution, for a pair of nubs)
d = reference diameter
b = span of nubs ($d \approx b$)
$S_{\exp}$ = exposed fin area (two nubs)
S = reference area ($\pi d^2/4$)

2. The term in the parenthesis takes into account the interference effects with the projectile body.

3. The lift force coefficient slope is obtained from

$$C_{L_\alpha} = K_{\text{int}_{ff}} C_{L_\alpha(nubpair)} \qquad \text{C-48}$$

4. The nub-nub interference effect (coefficient $K_{\text{int}_{ff}}$) is calculated from Equation E-11.

5. In case of projectile with 4 nubs the other pair is assumed here to be in horizontal level (and the other in vertical position) producing the lift according to the Equation C-47.

C.9.2 Pitching moment

The nubs effect on pitching moment coefficient slope is obtained by assuming the force center to be the nub plan form area center (x_{snubs}). The nubs effect on the pitch damping moment coefficient is estimated from

$$C_{mq} = -2C_{L_\alpha}\left(\frac{\Delta x}{d}\right)^2 \qquad \text{C-49}$$

where

Δx = arm length $(x_{cg} - x_{snubs})$

C.9.3 Magnus moment

1. The Magnus-moment coefficient slope $C_{n\alpha}$ is estimated for a **pair of nubs** from

$$C_{n\alpha_{nubpair}} = -\frac{8}{\pi}C_{N\alpha}\delta \qquad \text{For a pair of nubs} \qquad \text{C-50}$$

in which C_{N_α} is the normal force coefficient slope for **one nub** (here $C_{N_\alpha} \approx C_{L_\alpha}$, half of the value given by C-47). The moment value does not depend on the spin rate.

2. The total moment coefficient slope is

$$C_{n\alpha} = -\frac{4}{\pi}C_{L_\alpha}\delta \qquad \text{C-51}$$

where the C_{L_α} is obtained from C-48. The coefficient has no definition in the STANAG 4355.

C.9.4 Roll moment

1. The nubs produce some roll moment (coefficient slope C_{l_δ}) and on the other hand also cause some spin damping (C_{l_p}). **One nub** caused roll producing moment slope is estimated here by

$$C_{l_\delta} = \frac{C_{L_{\alpha_{nubpair}}}}{16} \qquad \text{One nub} \qquad \text{C-52}$$

2. The coefficient $C_{L\alpha}$ is the slope according to C-47 and it is divided here by 4 to make the result valid for a nub. Further more it is divided by two to take into account the smaller interference (proposed Slender Body Theory equation to be used for interference $1+\frac{d}{b}$) and once more to take into account the arm length *d*/2. The coefficient slope is obtained from

$$C_{l_\delta} = n_{nubs} C_{l_{\delta\, nub}} \qquad \text{C-53}$$

C.9.5 Spin damping

1. The spin damping moment coefficient C_{l_p} for the nubs only is estimated

$$\frac{C_{l\,p}}{C_{l_\delta}} = -2.15\frac{y_c}{d} \qquad \text{C-54}$$

where

y_c = arm length

2. The relation $\frac{y_c}{d}$ is about 0.45-0.5 and thus the total damping for nubs can be estimated from $C_{lp} \approx -C_{l\delta}$.

3. NATO STANAG 4355 standard definition for spin coefficient C_{Spin} is

$$C_{Spin} = \frac{C_{lp} + C_{l_\delta}\dfrac{\delta}{\left(\dfrac{pd}{2V}\right)}}{2} \qquad \text{C-55}$$

4. The spin damping moment coefficient C_{lp} is now the coefficient for the entire projectile.

INTENTIONALLY BLANK

ANNEX D DRAG COMPUTATION METHODS FOR PROJECTIOLE FINS

1. The zero angle of attack drag of a projectile consists of the individuals drags of the nose, cylindrical part, boat-tail/flare, tail boom, base, protuberances (driving band, grooves etc.), nubs and fins (see Figure 14). The corresponding drag coefficient C_{D_0} can be written as a sum of the following form:

$$C_{D_0} = C_{D_{body}} + C_{D\,fin} \qquad \text{D-1}$$

2. This Annex describes a simplified method to compute the drag coefficient $C_{D\,fin}$. The components of $C_{D_{body}}$ are discussed in Annex B.

3. The drag coefficient of fins ($C_{D\,fin}$) at zero angle of attack is computed in the presentation as a function of Mach number, but also some effect of Reynolds number is introduced via skin friction. The reference area is a circle area based on the diameter of the projectile cylindrical part. The fin drag of a projectile consists of the wave drag, blunt leading edge drag, blunt trailing edge drag and friction drag as a sum of the following form:

$$C_{D\,fin} = C_{D\,fin_{wave}} + C_{D\,fin_{LE}} + C_{D\,fin_{TE}} + C_{D\,fin_{viscous}} \qquad \text{D-2}$$

4. The subscripts *LE* and *TE* are for leading edge and trailing edge respectively.

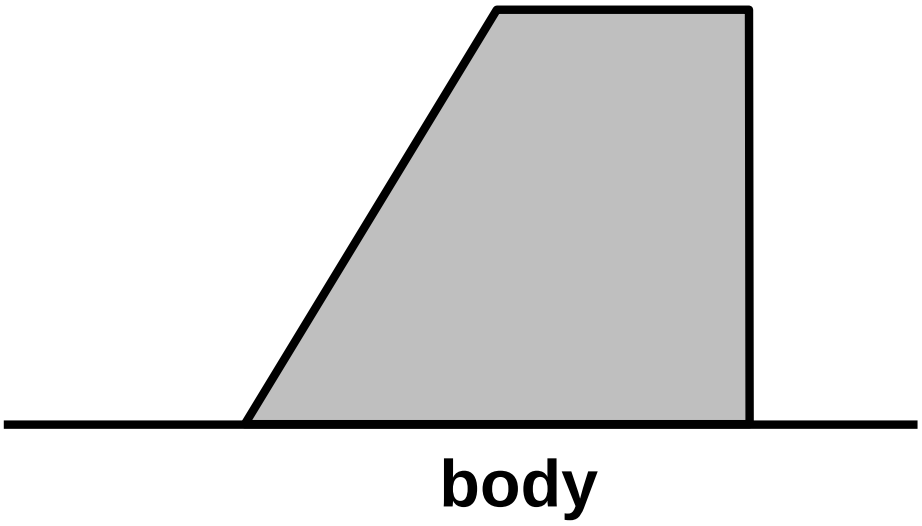

Figure 14: The fin is an individual panel in this chapter considering the drag computation. The wetted area of fin is the projected area S_{fin} as doubled.

D.1 WAVE DRAG

1. The wave drag at supersonic speeds for fins with sharp leading/tailing edges (see Figure 15) is calculated according to the equation D-3.

$$C_{D_{fin\ wave}} = n_{fin}\frac{K}{Ma}\left(\frac{t}{c}\right)^2_{av}\frac{S_{fin}}{S} \qquad \text{Supersonic leading edge} \qquad \text{D-3}$$

where

K = shape correction factor (see Figure 15)

$\left(\frac{t}{c}\right)_{av}$ = average fin thickness ratio

S = reference area ($\pi d^2/4$)

S_{fin} = fin area (see Figure 14)

$\Lambda_{LE_{fin}}$ = sweep angle, fin leading edge (see Figure 18)

n_{fin} = number of fins

2. The equation D-3 is applied when $Ma_{LE} \geq 1$ (Mach number normal to leading edge). Ma_{LE} is supersonic if $\mu > \Lambda_{LE_{fin}}$. The Mach angle μ is computed from

$$\mu = \arcsin\left(\frac{1}{Ma}\right) \qquad \text{D-4}$$

3. The drag value is taken to be constant down to free-stream Mach number 1 if $\mu < \Lambda_{LE_{fin}}$.

4. At subsonic region the drag goes linearly to zero at a Mach number estimated from equation D-5.

$$\left(\frac{t}{c}\right)_{av} = \left(\frac{\beta}{1.4}\right)^3 \qquad \text{D-5}$$

where

β = compressibility parameter ($\sqrt{|Ma^2 - 1|}$)

5. The fin thickness ratio $\left(\frac{t}{c}\right)_{av}$ is an average value without the blunt part contribution.

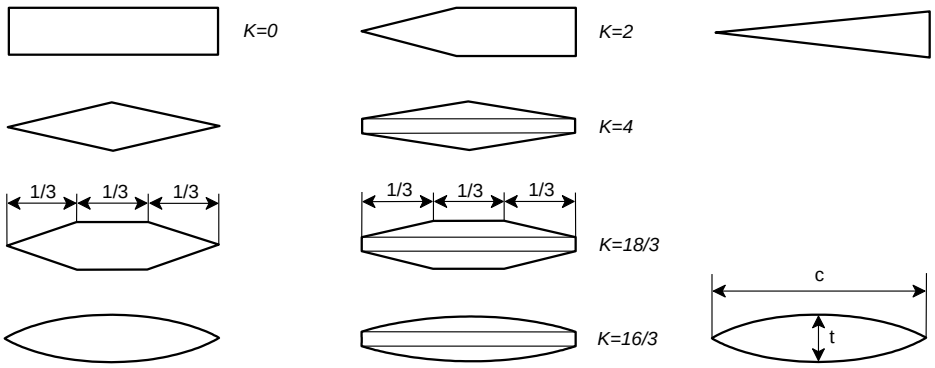

Figure 15: Airfoil shape correction factor *K* for a variety of airfoil geometries. The used thickness value t in the equation D-3 is the total thickness minus the blunt part contribution. $\left(\frac{t}{c}\right)_{av}$ is zero for a flat plate fin.

D.2 BLUNT LEADING EDGE DRAG

1. The **blunt leading edge** average pressure coefficient C_p is estimated by utilizing equations D-6 and D-7 .

$$C_p = \frac{1.25 k_1}{2} \quad \text{(see B-7)} \qquad 0 \le Ma < 1 \qquad \text{D-6}$$

$$C_p = k_1 \quad \text{(see B-8)} \qquad 1 \le Ma \qquad \text{D-7}$$

2. The **average** pressure coefficient on the surface of the fin blunt leading edge at **subsonic** speeds is estimated by dividing the obtained stagnation value ($\approx 1.25 k_1$) by 2.

3. The equation D-7 is applied for fins at supersonic speeds and subsequently, the leading edge sweep angle is taken into account by multiplying the result by $\cos^2 \Lambda_{LE_{fin}}$.

$$C_P = \cos^2 \Lambda_{LE_{fin}} C_p \quad \text{(see D-7)} \qquad \text{D-8}$$

4. Finally, the drag coefficient is obtained by multiplying C_P by the number of fins (n_{fin}), taking the reference area (*S*) and fin dimensions (Figure 16) into account.

$$C_{D_{fin_{LE}}} = C_P \frac{t_{LE}\, b_{fin}}{S} n_{fin} \qquad \text{D-9}$$

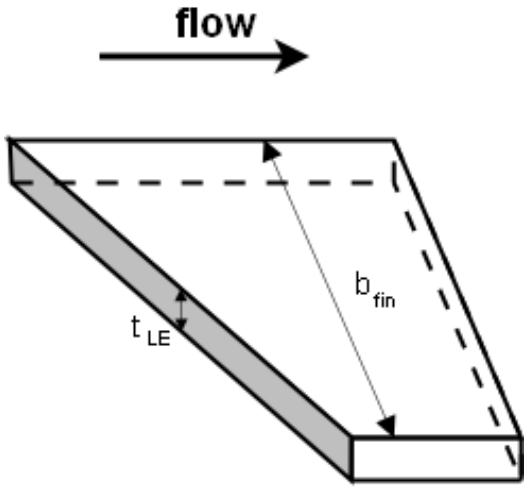

Figure 16: Schematic of fin blunt leading edge geometry.

D.3 BLUNT TRAILING EDGE DRAG

1. The average pressure coefficient on a fin blunt trailing edge is computed at subsonic and supersonic regions according to equations D-10 and D-11.

$$C_p = -\left(0.3 + \frac{Ma^4}{3}\right) \qquad Ma < 1 \qquad \text{D-10}$$

$$C_p = -0.65 Ma^{-1.68} \qquad Ma \geq 1 \qquad \text{D-11}$$

2. The trailing edge drag coefficient is obtained by multiplying it by the number of fins (n_{fin}), taking the reference area (S) and fin dimensions (Figure 17) into account.

$$C_{D_{fin\,TE}} = -C_p \frac{t_{TE}\, b_{fin}}{S} n_{fin} \qquad \text{D-12}$$

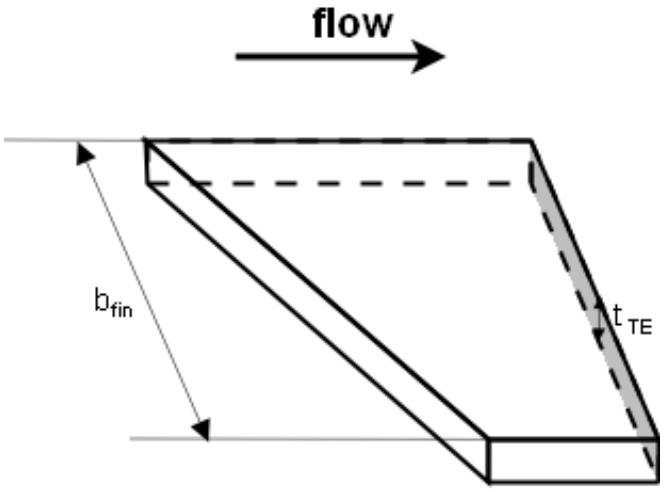

Figure 17: Schematic of fin blunt trailing edge geometry.

D.4 FRICTION DRAG

1. The fin friction drag is calculated by same equations (B-33 and B-34) as in projectile skin friction drag (see Annex B). In fin case S_{wetted} is the wetted surface area of fins, instead of the wetted surface area of projectile body (B-33) and flow is consider to be turbulent (B-34).

$$C_{D_f} = C_f \frac{S_{wetted}}{S} \qquad \text{D-13}$$

where

S_{wetted} = wetted surface area of fins ($2 * S_{fin} * n_{fin}$)

2. The turbulent skin friction coefficient C_f is computed by equation

$$C_f = \frac{0.455}{(\log \mathrm{Re}_{\bar{c}})^{2.58}} \left(1 + 0.21 Ma^2\right)^{-0.32} \qquad \text{D-14}$$

where

$\mathrm{Re}_{\bar{c}}$ = Reynolds number $= \frac{V\bar{c}}{\nu}$

$\bar{c}$ = Mean Aerodynamic Chord (MAC), (see Eq. E-4 and Figure 18)

ν = kinematic viscosity (see Equation B-36)

INTENTIONALLY BLANK

ANNEX E LIFT FORCE AND MOMENT COMPUTATION METHODS FINS

E.1 LIFT FORCE COMPUTATION

1. The wing lift force slope estimated in this chapter is valid at zero angle of attack. A projectile geometry with the nomenclature used is depicted in Figure 1.

2. The projectile total lift force coefficient slope is derived from computed zero normal force coefficient slope and projectile total zero angle of attack drag (Eq. E-1). The projectile total normal force coefficient slope is obtained as a sum of the component slopes (Eq. E-2).

$$C_{L_{\alpha_0}} = C_{N_{\alpha_0}} - C_{D_0} \qquad \text{E-1}$$

$$C_{N_{\alpha_0}} = \left[C_{N_{\alpha_0}}\right]_b + K_{\text{int}_{wb}} K_{\text{int}_{ff}} \left[C_{N_{\alpha_0}}\right]_w \qquad \text{E-2}$$

3. The methods to estimate the body normal force slope $\left[C_{N_{\alpha_0}}\right]_b$ are described in Annex C. The following chapters include the corresponding methods for fins.

E.2 WING LIFT SLOPE

1. A concept of exposed wing is introduced here. The exposed wing is obtained by joining two fins together (see Figure 18). The exposed wing normal force coefficient slope at zero angle of attack $\left[C_{N_{\alpha_0}}\right]_w$ is computed by

$$\left[C_{N_{\alpha_0}}\right]_w = \frac{2\pi A_{\text{exp}}}{2 + \left(A_{\text{exp}}{}^2\left(\beta^2 + \tan^2 \Lambda_{c/2}\right) + 4\right)^{1/2}} * \frac{S_{\text{exp}}}{S} \qquad \text{E-3}$$

where

A_{exp} = aspect ratio (exposed wing) $\left(\frac{b_{\text{exp}}^2}{S_{\text{exp}}}\right)$

$\Lambda_{c/2}$ = half chord sweep angle

S = reference area

S_{exp} = exposed wing area

β = $\sqrt{|Ma^2 - 1|}$

2. The sudden loss of lift at transonic area is a fairly complex phenomenon to predict and the following limitation is made to avoid overestimating the stability (lifting force) provided by wings through transonic region.

3. The coefficient value at transonic region is limited up to the value obtained at $Ma = 1 + \frac{\sqrt{A_{\exp}}}{10}$. The limited value is used whenever the result obtained from E-3 is larger than the limiting value.

4. Mean Aerodynamic Chord (MAC, $\bar{c}$) is computed from

$$\bar{c} = \frac{2}{3} c_r \frac{1 + \lambda + \lambda^2}{1 + \lambda} \qquad \text{E-4}$$

$$\lambda = \frac{c_t}{c_r} \qquad \text{E-5}$$

where

c_t = length of fin tip (see Figure 18)

c_r = length of fin root (see Figure 18)

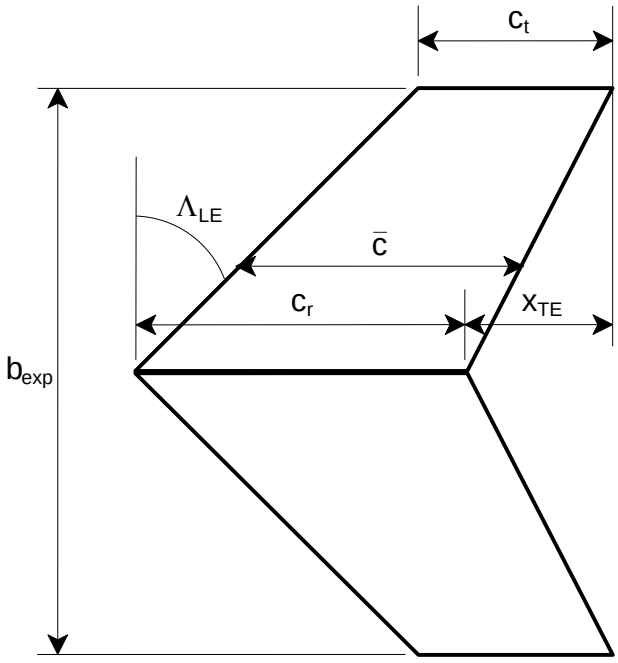

Figure 18: Exposed wing geometry without body. The equations E-14 and E-15 gives the aerodynamic center value behind the exposed wing apex point. Mean aerodynamic chord (MAC) is computed from equations E-4 and E-5.

E.3 FIN THICKNESS EFFECT

1. The **trailing edge thickness** increases the normal force coefficient slope and the increment $\Delta\left[C_{N_{\alpha_0}}\right]_w$ is computed by

$$\Delta\left[C_{N_{\alpha_0}}\right]_w = \left[C_{N_{\alpha_0}}\right]_w \left(1.2\left(\frac{t_{TE}}{\bar{c}}\right) - 1.2\left(\frac{t_{TE}}{\bar{c}}\right)^2\right) \qquad \text{E-6}$$

where

$\left[C_{N_{\alpha_0}}\right]_w$ = normal force coefficient slope at zero angle of attack

t_{TE} = trailing edge thickness

$\bar{c}$ = mean aerodynamic chord (MAC)

2. The equation is used here to estimate the thickness effect on **normal force slope**. The second order term is included to the equation to make the effect vanish if the fin trailing edge thickness t_{TE} was increased excessively.

3. The leading edge thickness also increases the slope, and the effect is obtained from equation

$$\Delta\left[C_{N_{\alpha_0}}\right]_w = \left[C_{N_{\alpha_0}}\right]_w \left(4.5\left(\frac{t_{LE}}{\bar{c}}\right)/Ma - 4.5\left(\frac{t_{LE}}{\bar{c}}\right)^2/Ma\right) \qquad \text{E-7}$$

where

t_{LE} = leading edge thickness

4. The Mach number in the equation is taken to be 1 at subsonic region. The equation was formulated to resemble the one handling the trailing edge thickness (Eq. E-6), assuming the accuracy and applicability to be corresponding. The second order term is included to the equation to make the blunting effect to vanish in case of extremely blunt fin sections.

E.4 INTERFERENCE EFFECTS

1. The aerodynamics of projectile components are estimated separately and summed up in the present method. However, in practice there are inter-dependences which are introduced via interference coefficients. The equations introduced here are used to estimate the zero angle of attack inter-dependences.

2. The wing-body interference coefficient is estimated from Slender Body Theory equation

$$K_{\text{int}_{wb}} = \left(1 + \frac{d}{b}\right)^2 \qquad \text{E-8}$$

where

d = projectile body diameter

b = total span including the body diameter

$K_{\text{int}\,wb} = K_{W_{(B)}} + K_{B_{(W)}}$ (or $K_W + K_B$), Wing in the presence of Body and Body in the presence of Wing at α = 0 and δ = 0 degrees

3. The carryover effect interference coefficient K_B is estimated based on the Slender Body Theory and linear-theory-based curves.

4. In the former method the sum of coefficients $K_W + K_B$ is obtained from E-8. Then the K_W is estimated from

$$K_W \approx 1 + \frac{d}{b} \qquad \text{E-9}$$

and the K_B is finally computed by subtracting K_W from the coefficient sum.

$$K_B = K_{\text{int}_{wb}} - K_W \qquad \text{E-10}$$

5. The interference coefficient values for a swept-back case are obtained from equations

$$K_B(sweptbackTE) = K_B \frac{c_r}{c_r + x_{TE}} \qquad \text{3-1}$$

$$K_W(sweptbackTE) = 1 + (K_W - 1)\frac{c_r}{c_r + x_{TE}} \qquad \text{3-2}$$

6. The sweptback trailing edge length x_{TE} is depicted in Figure 18.

7. The latter-mentioned method is used at supersonic speeds in case $A_e\sqrt{Ma^2 - 1} > 1$. The length of the body (carryover effect on the body) behind the fin set is taken into account by simply interpolating linearly between the curve-obtained values for “no body behind fins” and “infinite length body behind fins”. The carry-over length is computed based on the Mach angle and body local diameter (see Figure 17).

8. The value of K_B is limited up to the result given by the Slender Body Theory.

9. The separate interference coefficients K_W and K_B are needed when the effect of angle of attack to aerodynamics is computed for a wing-body combination.

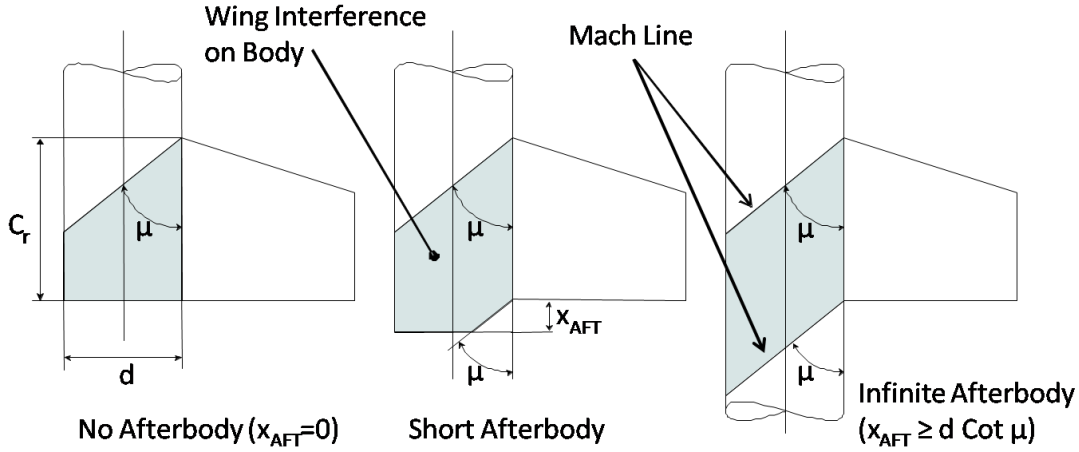

Figure 19: Determination of wing influence on body at supersonic speeds.

7. The fin-fin interference of a fin set is estimated here from equation

$$K_{\mathrm{int}_{ff}} = k\left(0.2\left(1+n_{fin}\right)\right) \qquad \text{E-11}$$

where

n_{fin} = number of fins in the group

k = 0.9, when Ma ≤ 1.2 and more than 6 fins
= 1 otherwise

8. The interference value is limited up to value 2. The assumption made here is that maximum number of fins is, in practice, 10 and increasing the number will not cause any more favorable lift force. The interference coefficient value 1 is used if the number of fins is 2 (horizontal wings).

9. The interference effects are taken into account by multiplying the obtained slope value $\left[C_{N\alpha_0}\right]_w$ for an exposed wing by the interference coefficients (see equation E-2).

10. The wing-body interference coefficient is further modified to include the effect of fin-body gaps and the effect of short body behind the fins.

E.5 FIN-BODY GAPS

1. The stream wise fin-body gaps cause loss of normal force and the phenomenon is taken into account via the value of interference coefficients. The interference

coefficients take into account the effect of body presence on wing aerodynamics and vice versa. The sum of fin-body interference coefficients $K_{\text{int}_{wb}} = K_W + K_B$ is multiplied by loss factor *FNF* to take into account the losses while normal force is estimated.

2. The loss factor is calculated from

$$FNF = 1 - 0.85k\sqrt{\frac{g}{d}} \qquad \text{E-12}$$

3. The symbol g is for gap width and d is the local body diameter (see Figure 20). The coefficient k takes into account the Mach number effect and $k = \sqrt{Ma}$ when Ma < 1 and goes linearly from value 1 to 0 when Mach number varies from 2 to 5. The coefficient value of k is 1 when 1 < Ma < 2 and k is 0 when Ma > 5.

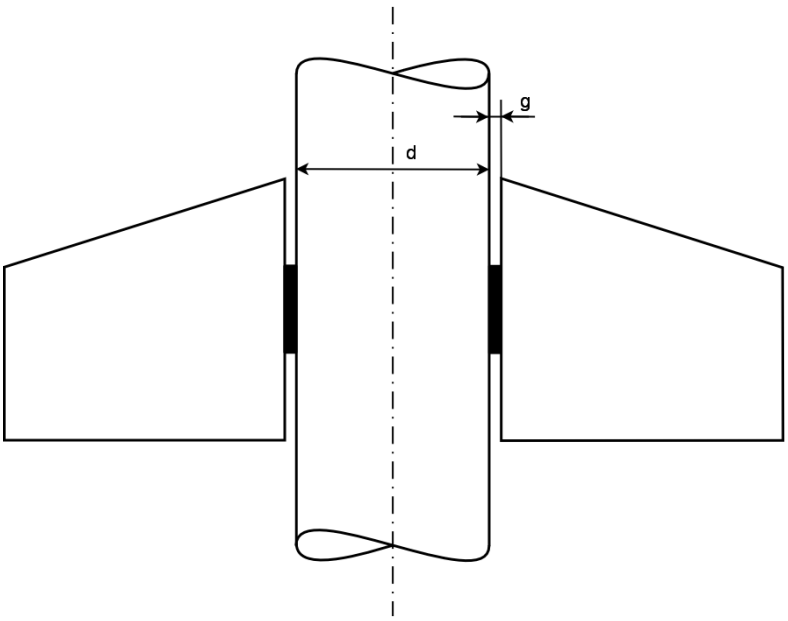

Figure 20: Gap(g) between fin and body.

4. The loss coefficient FNF is further modified by removing the K_W contribution from the losses. The interference loss due to gaps is assumed to have just an effect entirely on the body carry-over, and the body effect on fin aerodynamics is assumed not to change due to the presence of relatively narrow gaps. The new loss coefficient $FNF1$ is estimated simply using zero angle of attack values for K_W and K_B and assuming the following ratio valid

$$FNF * (K_W + K_B) = FNF1 * K_B + K_W \qquad \text{E-13}$$

5. The minimum allowable value of $FNF1$ is set to be 0.

E.6 AERODYNAMIC CENTER

1. The aerodynamic center of an exposed wing (behind the wing apex point) is estimated at supersonic and transonic speeds from

$$x_{ac} = 0.7c_r - 0.2c_t + 0.4x_{TE} - k\frac{\bar{c}}{4} \qquad Ma > 1 \qquad \text{E-14}$$

$$k = \left(\frac{1}{Ma}\right)^{A_{\exp}} \qquad \text{E-15}$$

where

$A_{\exp}$ = aspect ratio of exposed wing

2. At subsonic speed, the coefficient *k* is 1 and the aerodynamic center is estimated from

$$x_{ac} = 0.7c_r - 0.2c_t + 0.4x_{TE} - \frac{\bar{c}}{4} \qquad Ma < 1 \qquad \text{E-16}$$

3. The equation for *k* shifts the center backwards with increasing Mach number. The backward shift of the center with increasing speed takes place moderately in case of small aspect ratio wings.

4. The contributions of fins to the pitching moment coefficient slope $C_{m_{\alpha_0}}$ are obtained by multiplying the dimensionless arm length by $\left[C_{N_{\alpha_0}}\right]_w$. The arm length between a reference point (center of gravity) and the wing aerodynamic center is made dimensionless by dividing it by body diameter *d*. Finally, the projectile total $C_{m_{\alpha_0}}$ value is obtained by summing the body and wing contributions.

$$C_{m_{\alpha_0}} = \left[C_{m_{\alpha_0}}\right]_b + \left[C_{N_{\alpha_0}}\right]_w \frac{\Delta x}{d} \qquad \text{E-17}$$

E.7 PITCH DAMPING MOMENT

1. The pitch damping moment caused by fins is computed from equation

$$C_{m_q} + C_{m_\alpha} = -2K_{\text{int}_{wb}} K_{\text{int}_{ff}} \left[C_{N_{\alpha_0}}\right]_w \left(\frac{\Delta x}{d}\right)^2 \qquad \text{E-18}$$

where

$C_{m_q} + C_{m_\alpha}$ = sum of pitch damping moment coefficients

$\left[C_{N_{\alpha_0}}\right]_w$ = normal force coefficient slope

Δx = distance between the center of gravity and the fin aerodynamic center

d = projectile body diameter

2. The projectile total pitch damping moment coefficient is obtained by summing up the body and fin contributions.

E.8 ROLLING MOMENT COEFFICIENTS

1. The roll-producing moment coefficient is obtained from the equation

$$C_{l_0} = n_{fin} \frac{\left[C_{N_{a_0}}\right]_w}{4} \delta_{eff} \frac{y_{arm}}{d} \qquad \text{E-19}$$

where n_{fin} is the number of fins and δ_{eff} is the fin effective cant angle (see Figure 21)

$$\delta_{eff} = \delta_{basic} + \delta_{bevel} \qquad \text{E-20}$$

2. The moment arm y_{arm} is estimated from

$$y_{arm} = \frac{r_{loc}}{2} + 0.9\frac{b_{\exp}}{2}\left[0.333 + 0.167\left(\frac{c_t}{c_r}\right)^{1/4}\right] \qquad \text{E-21}$$

3. The moment arm from centerline depends on the local body radius r_{loc}, fin exposed span $b_{\exp}$ and fin taper ratio. The fin contribution to the arm length is decreased by amount of 10% due to estimated tip effects. The wing normal force coefficient slope $\left[C_{N_{\alpha 0}}\right]_w$ for exposed wing includes no wing-body interference effects.

4. The basic and effective cant angle definitions are depicted in Figure 21. The beveling effect is applied without leading edge contribution in case of a subsonic leading edge. The rolling-moment-producing term of a subsonic rounded leading edge might even be reversed compared to the case of a supersonic leading edge. The other compressibility effects on the rolling moment are assumed to be taken into account in the value of wing normal force.

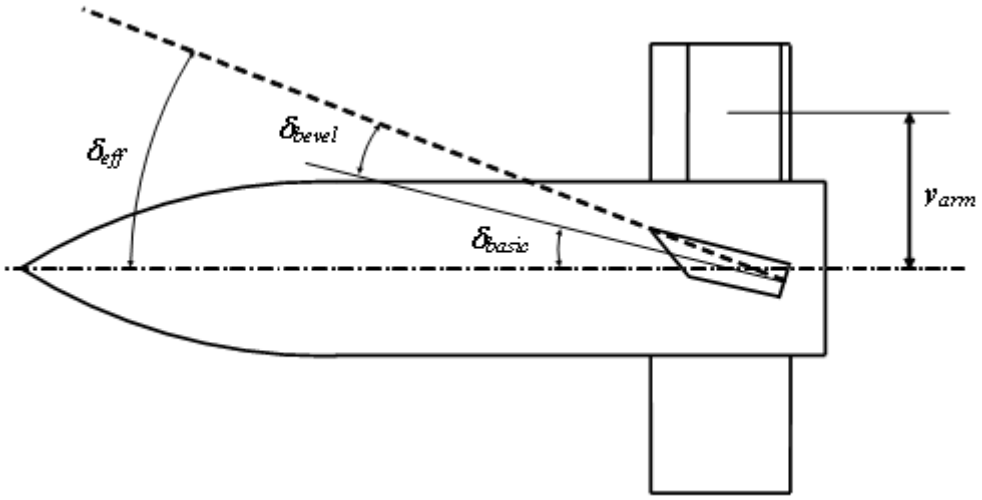

Figure 21: Geometry definition of basic cant angle δ_{basic} and cant angle of asymmetrical fin δ_{bevel}. The positive cant angle δ causes a clockwise spin seen from behind of projectile.

5. The spin-damping moment coefficient $C_{l\hat{p}}$ is obtained from

$$C_{l\hat{p}} = -2.15 \frac{C_{l_0}}{\delta_{eff}} \frac{y_{arm}}{d} \qquad \text{E-22}$$

6. The spin damping moment coefficient is obtained **only** for fins having some cant angle or asymmetry ($C_{l_0} \neq 0$).

7. The roll-producing moment coefficient applied in the formula E-23 is now based on the local diameter as well as the damping coefficient obtained. The roll-producing moment coefficient with the proper reference system is obtained from

$$C_{lo} = C_{lo} \frac{d_{loc}}{d} \qquad \text{E-23}$$

8. The spin-damping moment coefficient is finally obtained from

$$C_{l\hat{p}} = C_{l\hat{p}} \frac{2y_{arm}}{d} \qquad \text{E-24}$$

E.9 MAGNUS PHENOMENON

1. The mechanism causing aerodynamic interaction between the projectile pitch and yaw planes is typically called the Magnus phenomenon. There are several origins for the interaction found and the one caused by fin cant angle/shape asymmetry is included into the methods described here. The Magnus effects for the body were described in Annex C.

2. A tilted normal force N_1 arises from the canted fin (see Figure 22) creating a sidewise (in yaw plane) turning moment with increasing angle of attack α in pitch plane.

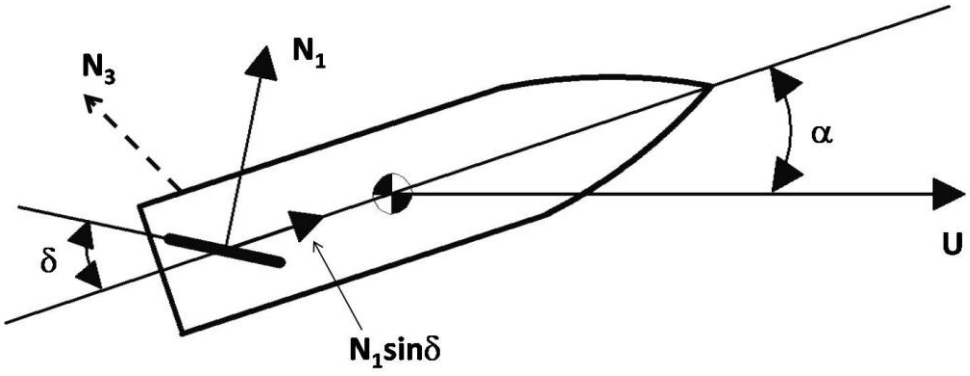

Figure 22: Nomenclature and origin of interaction. The fin normal forces N_1 and N_3 (from fin in opposite side) are not parallel due to fin cant angle δ.

3. The Magnus moment (turning the nose left to negative direction if positive cant angle) is determined from

$$C_{n_\alpha} = -\left(\frac{8}{\pi}\right) K_{\mathrm{int}_{wb}} K_{\mathrm{int}_{ff}} \left[C_{N_{\alpha 0}}\right]_w \delta_{eff} \qquad \text{E-25}$$

where

$$\delta_{eff} = \delta_{basic} + \delta_{bevel}$$

$$\delta_{bevel} = \delta_{bevel_0} \cos\left(\frac{\mu}{A_{\exp}}\right)$$ (the term $\left(\frac{\mu}{A_{\exp}}\right)$ is limited here up to $\frac{\pi}{2}$)

4. The positive cant angle δ causes a clockwise spin seen from behind of the projectile. The symbol μ ($\mu = \arcsin\frac{1}{Ma}$) denotes the Mach angle (see Figure 23) and A_{exp} is the aspect ratio of exposed wing (a fin pair without body contribution, see Figure 18). The 3-dimensional flow effects on the bevelings are small according to the equation if the Mach number and/or the aspect ratio are large. The sweep-angle effects are not taken into account.

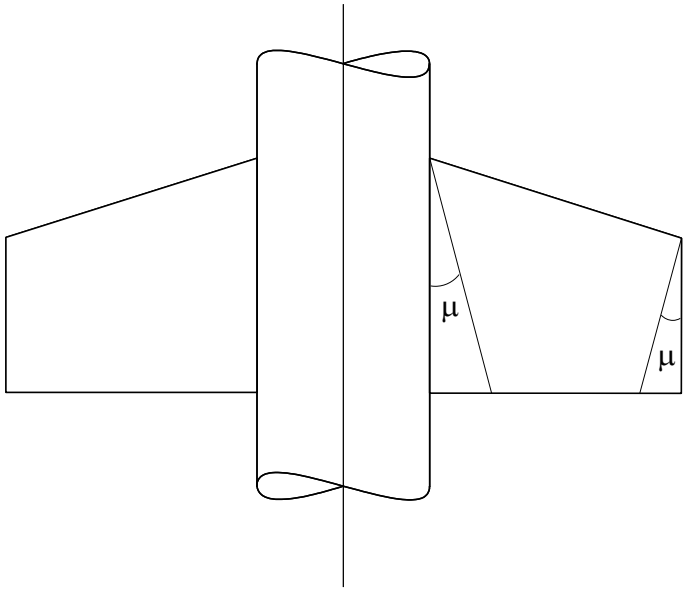

Figure 23: The flow is affected by fin-tip and body-junction effects inside the Mach angle μ.

INTENTIONALLY BLANK

ANNEX F GENERALISED YAW AERODYNAMICS

F.1 FORMULATION OF COEFFICIENTS

1. The angle of attack α is defined to be an angle between the projectile symmetry axis and the velocity vector as depicted in Figure 24.

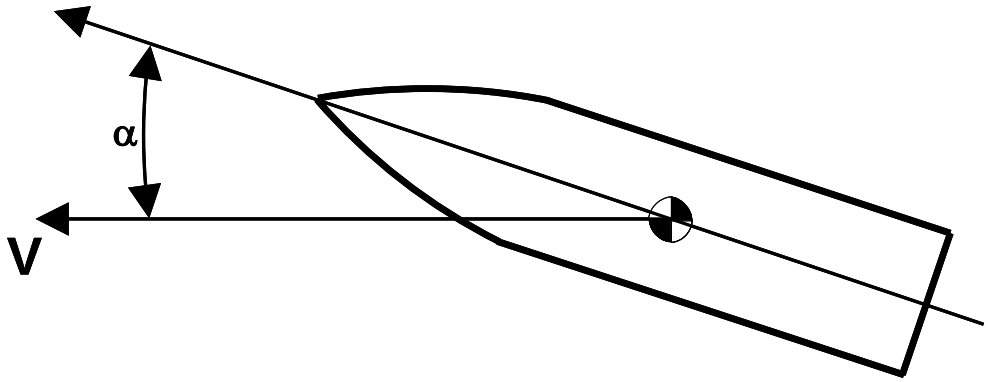

Figure 24: The definition of angle of attack α.

2. The effect of angle of attack α on aerodynamics is expressed in form

$$C_D = C_{D_0} + C_{D_{\alpha^2}}\alpha^2 \qquad \text{F-1}$$

$$C_{L_\alpha} = C_{L_{\alpha_0}} + C_{L_{\alpha^3}}\alpha^2 \qquad \text{F-2}$$

$$C_{m_\alpha} = C_{m_{\alpha_0}} + C_{m_{\alpha^3}}\alpha^2 \qquad \text{F-3}$$

3. The subscript 0 is for the value at zero angle of attack. The effect of angle of attack will be taken into account only for the three coefficients presented in Equations F-1 to F-3 above.

4. The emphasis is to make the polynomial fits to give the best approximations for coefficients at angle of attack at about 15 degrees. However, the equations F-1 to F-3 give reasonable estimates for aerodynamics up to angle of attack 30 degrees. The methods presented here are valid for a wing-body combination but are also applied for a body only.

5. The drag and lift angle of attack dependence is computed based on the corresponding behavior of the axial and normal force coefficients.

6. The higher order terms $C_{D_{\alpha^2}}, C_{L_{\alpha^3}} \text{ and } C_{m_{\alpha^3}}$ for the Equations F-1…F-3 are calculated from the C_N and C_A curves.

7. The C_N and C_A are computed according to Equations F-6 and F-16. The C_D and C_L are obtained from

$$C_D = C_A \cos\alpha + C_N \sin\alpha \qquad \text{F-4}$$

$$C_L = C_N \cos\alpha - C_A \sin\alpha \qquad \text{F-5}$$

8. The coefficient $C_{D_{\alpha^2}}$ is solved at angle of attack α = 20 degrees based on the known values of C_D at 0 and 20 degrees (see Eq. F-1). The other coefficients $C_{L_{\alpha^3}}$ and $C_{m_{\alpha^3}}$ are obtained in the similar manner.

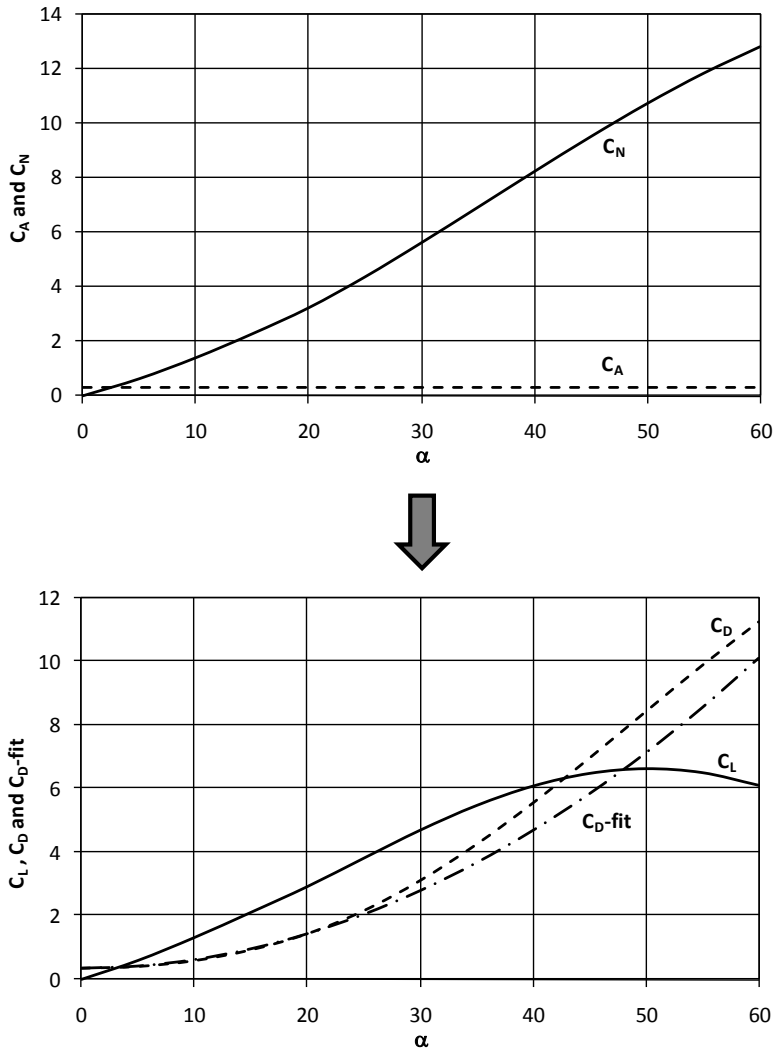

Figure 25: Computed C_A and C_N transformed to C_L, C_D and $C_D - fit$. $C_{D_{\alpha^2}}$ is solved using Eq. F-1 at $\alpha = 0°$ and $\alpha = 20°$ ($C_D - fit$ curve).

F.2 NORMAL FORCE

1. For a fin-stabilized projectile, the entire normal force coefficient is obtained from

$$C_N = C_{NB} + C_{NW(B)} + C_{NB(W)} \qquad \text{F-6}$$

where C_{NB} is the body alone normal force coefficient, $C_{NW(B)}$ the wing normal force coefficient in the presence of a body and $C_{NB(W)}$ the body normal force coefficient in the presence of a wing (body carryover).

2. The **body alone normal force** coefficient as a function of angle of attack is computed based on the cross-flow theory equation

$$C_{NB} = \left[C_{N_{\alpha_0}}\right]_b \cos\alpha \sin\alpha + \eta \bar{c}_{dc} \sin^2\alpha \frac{S_c}{S} \qquad \text{F-7}$$

where

$\left[C_{N_{\alpha_0}}\right]_b$ = body normal force coefficient slope at zero angle of attack

α = angle of attack

η = the ratio of the cross-flow drag on a finite cylinder to the drag of an infinite cylinder $= \begin{cases} 0.5, Ma < 1 \\ 1.0, Ma \geq 1 \end{cases}$

$\bar{c}_{dc}$ = cross-flow drag coefficient $= \begin{cases} 0.6, Ma < 1 \\ 1.2, Ma \geq 1 \end{cases}$

3. **The wing normal force** coefficient in the presence of body $C_{NW(B)}$ is estimated using a concept of an equivalent angle of attack α_{eq} which is computed from

$$\alpha_{eq} = K_W \alpha + k_W \delta \qquad \text{F-8}$$

where

α = angle of attack

δ = control deflection

K_W, k_W = interference factors (body influence on wing aerodynamics when $\alpha \neq 0$, $\delta = 0$ (K_W) and $\alpha = 0$, $\delta \neq 0$ (k_W))

4. Furthermore, $C_{NW(B)}$ is equal to C_{NW} evaluated at α_{eq} :

$$C_{NW(B)} = C_{NW}(\alpha_{eq}) \qquad \text{F-9}$$

5. The coefficient C_{NW} for a **exposed wing** (see Figure 26) is estimated from equation

$$C_{NW} = \left[C_{N_{\alpha_0}}\right]_w \sin(\alpha)\cos(\alpha) + \sin^2(\alpha)\ \frac{S_{\exp}}{S} \qquad \text{F-10}$$

6. The coefficient $C_{NW(B)}$ including the control effects is now obtained if α is replaced by α_{eq} in Eq. F-10. The slope value in the equation is already properly referenced.

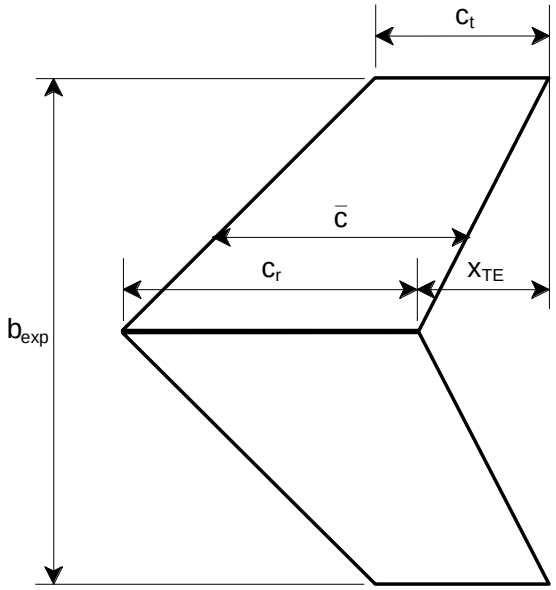

Figure 26: Exposed wing geometry (= 2 fins together without body contribution).

7. The wing normal force coefficient C_{NW} is limited up to values 1.2 and 1.5 at subsonic and supersonic speeds respectively (reference area is wing exposed area while the limit checked).

8. The interference factors K_W and k_W are computed based on closed form equations from the Slender Body Theory (SBT). The interference coefficient K_W is also made variable with the angle of attack according to relation

$$K_W(\alpha) = (K_{W_0} - 1)(0.6 - \sin(\alpha)Ma)/0.6 + 1 \qquad \text{F-11}$$

9. The notation K_{W0} means the coefficient value at zero angle of attack α. The coefficient minimum $K_W(\alpha)$ value is set to be 0.9.

10. The behavior of interference coefficient k_W as a function of Ma, α and δ is simply varied according to equation

$$k_W(\alpha,\delta) = k_{W0}\cos(\alpha+\delta) \qquad \text{F-12}$$

11. The notation k_{W0} stands for the coefficient value at zero α and δ. The coefficient value is taken to be 1.

12. The corresponding **carryover normal force to body** in the presence of a wing is estimated from equation

$$C_{NB(W)} = C_{roll_N}\frac{K_B(\alpha=0)}{K_W(\alpha=0)}C_{NW(B)}\cos(\delta) \qquad \text{F-13}$$

13. The interference coefficients K_W and K_B are calculated from Equations E-9 and E-10. If the fin-body gaps are included in the calculations, the coefficient K_B is multiplied with the loss coefficient $FNF1$ from Equation E-13 before calculating the $C_{NB(W)}$.

14. The carryover, obtained from F-13, is further multiplied by $\cos\delta$ if fin-body gaps are present.

15. The body carryover force $C_{NB(W)}$ is computed using the zero angle values for the ratio of interference coefficients K_B/K_W. The nonlinearities are assumed to be taken into account in the value of $C_{NW(B)}$ (See Eq. F-13).

16. The **roll position** affects the body carryover phenomena and a lot of normal force is lost when the body is rolled from ⊕-position to ⊗-position (bank angle 45 degrees, see Figure 27). This effect is taken into account in the value of C_{roll_N} coefficient (at ⊗-position). The C_{roll_N} term was included into the equation and is 1 in case of ⊕-roll position.

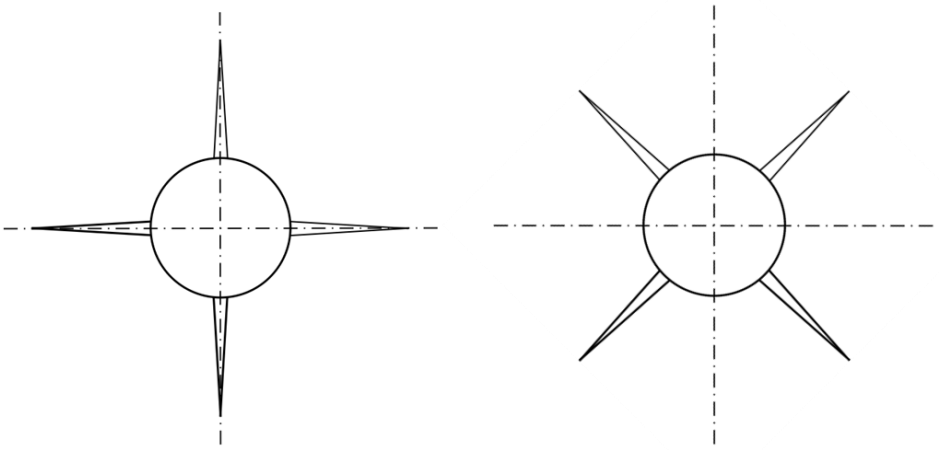

Figure 27: Projectile roll position (⊕-roll position at left and ⊗-roll position at right).

17. The roll coefficient C_{roll_N} was made variable with the angle of attack α according to

$$C_{roll_N} = \frac{0.6 - \frac{4}{n_{fin}}\sin(\alpha)Ma}{0.6} \qquad \text{F-14}$$

18. The term $4/n_{fin}$ (1 in case of four fins) makes the roll position effect on the body carryover to get smaller in case of multi-fin projectiles ($C_{roll_N} \to 1$ when $n_{fin} \to \infty$). The minimum value of coefficient C_{roll_N} is set to be 0.

19. The Mach number used in the equations is limited to the minimum value of 0.8 when K_W and C_{roll_N} are computed in order to make the angle of attack effect on interference resemble the one at higher Mach numbers.

20. The fin-fin interference $K_{\inf ffo}$ at zero angle of attack is computed according to Annex D and is used to correct projectile aerodynamics if more than four fins are present. An interference coefficient $K_{\inf ff}(\alpha)$ is estimated from equation

$$K_{\inf ff} = 1 + (K_{\inf ff_0} - 1) * \cos(2\alpha) \qquad \text{F-15}$$

21. The equation F-15 simply assumes that the extra normal force caused by multiple fins vanishes when $\alpha \geq 45°$.

F.3 AXIAL FORCE

1. In the subsonic region, the **axial-force** coefficient for **the entire projectile** is estimated based on the cross-flow drag theory from equation

$$C_A(\alpha) = C_{A_0} \cos^2 \alpha \qquad Ma < 1 \qquad \text{F-16}$$

2. The axial force coefficient at zero angle of attack C_{A_0} is obtained according to the methods described in Annex B ($C_{A_0} = C_{D_0}$). At supersonic speeds, the coefficient $C_A\ f(\alpha)$ is taken to be constant.

$$C_A(\alpha) = C_{A_0} \qquad Ma > 1 \qquad \text{F-17}$$

3. The contribution of control deflection to the axial force coefficient is estimated here from

$$C_A(\delta) = C_{roll_A} \sin(\delta) C_{NW(B)} \qquad \text{F-18}$$

where

C_{roll_A} = 1, when ⊕ - roll position

C_{roll_A} = 2, when ⊗ - roll position

4. The coefficient C_{roll_A} takes into account the roll position effect on the axial force. Its value is 1 in case of ⊕-position (2 horizontal fins are assumed to be deflected) and in case of ⊗-position, the coefficient value is 2 since **four fins** are assumed to be deflected with equal amount δ to create a corresponding normal force in the pitch plane.

F.4 PITCHING MOMENT

The normal force coefficient C_{N90} at the yaw angle 90° is obtained from equation F-7 and the corresponding moment coefficient is computed from equation

$$C_{m90} = \frac{C_{N90}(x_{cg} - x_{CrossAreaCenter})}{d} \qquad \text{F-19}$$

The body pitching moment yaw trend is obtained from

$$C_m = C_{m_{\alpha 0}} * \alpha * (\cos\alpha)^2 + (\sin\alpha)^2 * C_{m90} \qquad \text{F-20}$$

2. The **wing** contribution to the pitching moment coefficient is estimated based on the normal force coefficient behaviour described in the text earlier. The center of

pressure is assumed to move backwards from its value at zero angle of attack with increasing angle of attack according to equation

$$x_{cp} = x_{cp0} + \sin|\alpha + \delta|(x_{cp90} - x_{cp0}) \qquad \text{F-21}$$

3. The limiting values for center of pressure at 0 and 90 degrees are computed according to Annex E. The latter is estimated using value 0 for the coefficient *k*, equation E-15. The equation F-21 is used for a projectile at ⊕-roll position.

4. The backward shift of the center of pressure with increasing wing angle of attack takes place more moderately in case of ⊗-roll position at all Mach numbers. The difference is largest at moderate angles and the ⊕ and ⊗–roll position centers of pressure are the same at wing angle of attack 0 and 90 degrees. The equation F-22 with $\sin(\alpha)$ raised to an exponent (2 in case of four fins) gives a behaviour resembling the describtion. The term $4/n_{fin}$ included (1 in case of four fins) makes the roll position effect to get smaller in case of a multi-fin projectile.

$$x_{cp} = x_{cp0} + \left[\sin|\alpha + \delta|\right]^{(1+4/n_{fin})}(x_{cp90} - x_{cp0}) \qquad \text{F-22}$$

5. The **entire projectile pitching** moment coefficient is obtained by summing up the wing and body contributions. The control effects are given assuming 2 horizontal fins to be deflected and the body bank angle is zero (+ attitude). The number of fins of each fin set has no effect on control deflection effect.

ANNEX G SELECTED BIBLIOGRAPHY

[1] **Sailaranta, T.** and **Siltavuori, A.,**
AeroFi – Technical Report, rev. 5.3.0.
Aero RD Ltd, Report T-2, 2013.

[2] **NATO**, STANAG 4355-The Modified Point Mass Trajectory Model.
Military Agency for Standardization (MAS), January 1997.

[3] **Hoerner, S. F**.,
Fluid-Dynamic Drag.
published by the Author, 1965.

[4] **Moore, F. G.,**
Approximate Methods for Weapon Aerodynamics.
Progress in Astronautics and Aeronautics Series, vol. 186, AIAA, 2000.

[5] **Luckert, H-J.,**
Static Stability and Drag Studies for Bodies of Revolution in Supersonic Flow.
AIAA Journal of Spacecraft and Rockets, Vol. 10, No. 11, November 1973.

[6] **MIL-HDBK-762**
Design of Aerodynamically Stabilized Free Rockets,
US Army Missile Command, July 1990.

[7] **Stoney, W. E. Jr**,
Collection of zero-lift drag data on bodies of revolution from free-flight investigations.
NASA, Technical Report R-100, USA, 1961.

[8] **Tanner, M,**
Steady base flows.
Progress in Aerospace Sciences, Vol. 21, 1984.

[9] **McCoy, R. L.**,
Estimation of the Static Aerodynamic Characteristics of Ordnance Projectiles at Supersonic Speeds.

Report 1682 Ballistic Research Laboratory, Aberdeen Proving Ground, Maryland, November 1973.

[10] **Charters, A. L.** and **Kent, R. H.**,
The Relation Between the Skin Friction Drag and the Spin Reducing Torque.
Report 287 Ballistic Research Laboratory, Aberdeen Proving Ground, Maryland, July 1942.

[11] **Hendry, C.E.**,
Contract MW22B/807 – Aerodynamics of Long Projectiles – Final Report, Part 2.
British Aerospace PLC, Dynamics Group, Sowerby Research Center, Bristol, England, UK, Report JS10134, Aug. 1984.

[12] **Mikhail, A. G.,**
Drag Correlation and Predictions of Surface Groove Drag for Kinetic Energy Projectiles.
Journal of Spacecraft and Rockets, vol. 26, no 5, AIAA, sept-oct 1989.

[13] **Janiga, P., Simard, M.** and **Lebegern, C.,**
Substantiation of Swedish base bleed model using 155 mm ERFB (NR265) base bleed projectile range data obtained from firings of cannons up to 52 calibers in length.
ADPA, 14th International Symposium on Ballistics, Quebec, Canada, 1993.

[14] **USAF Stability And Control DATCOM.**
Published by Flight Control Division, Air Force Flight Dynamics Laboratory. Revised edition. Wright-Patterson Air Force Base, Ohio, 1978.

[15] **Ericsson, L. E.**,
Effect of Mach Number on Slender Vehicle Dynamics.
Journal of Spacecraft, Vol.18 No.1, January-February 1981.

[16] **Chin, S., S**.,
Missile configuration design.
McGraw-Hill Book Company, 1961.

[17] **Platou, A. S.**,
Magnus characteristics of finned and nonfinned projectiles.
AIAA Journal. vol. 3, no. 1, AIAA, January 1965.

[18] **Mikhail, A. G.,**
Roll damping coefficient prediction for finned projectiles.
Proceedings vol. 1, 14th International Symposium on Ballistics, Quebec, Canada, ADPA, 1993.

[19] **Mendenhall, M. R. (ed),**
Tactical Missile Aerodynamics : Prediction methodology.
Progress in Astronautics and Aeronautics Series, Vol. 142, AIAA, 1992.

[20] **Hemsch, M. J. (ed),**
Tactical Missile Aerodynamics : General Topics.
Progress in Astronautics and Aeronautics Series, Vol. 141, AIAA, 1992.

[21] **Sigal, A.** and **Victor, M.,**
The effects of cross-section shape on the aerodynamic characteristics of fins at supersonic Mach numbers.
Proceedings vol. 3, 15th International Symposium on Ballistics, Jerusalem, Israel, 1995.

[22] **Fagerström, B.; Kilpeläinen, J.** and **Laine, S.**,
A study of bluntness effects on the performance of projectile fins using tests of oversize low-speed wind tunnel models.
Proceedings vol. 2, 16th International Symposium on Ballistics, San Francisco, USA, 1996.

[23] **Fagerström, B.; Kemppainen, P.** and **Sailaranta, T.**,
Bluntness effects on thick projectile fins at transonic and moderate supersonic speeds.
Proceedings vol. 1, 17th International Symposium on Ballistics, Miranda, South Africa, 1998.

[24] **Mikhail, A. G.,**
Fin gaps and body slots - Effects and modeling for projectiles and missiles.

AIAA, Journal of Spacecraft and Rockets, vol. 25, no. 5, September-October 1988.

[25] **Mikhail, A. G.,**
Lift losses for fin-body gaps in transonic and supersonic speeds.
AIAA, Journal of Spacecraft and Rockets, vol. 27, no. 6, November-December 1990.

[26] **Mikhail, A. G.,**
Fin gaps and body slots - Effects and modeling for projectiles and missiles.
AIAA, Journal of Spacecraft and Rockets, vol. 25, no. 5, September-October 1988.

[27] **Mikhail, A. G.,**
Lift losses for fin-body gaps in transonic and supersonic speeds.
AIAA, Journal of Spacecraft and Rockets, vol. 27, no. 6, November-December 1990.

[28] **Zarchan, P.,**
Tactical and Strategic Missile Guidance, Third Edition.
Progress in Astronautics and Aeronautics, vol. 176, AIAA, 1998.

[29] **Fleeman, E., L.,**
Tactical Missile Design.
Education Series, AIAA, 2001.

[30] **Benton, E. R.**,
Supersonic Magnus Effect on a Finned Missile.
AIAA Journal. vol. 2, no. 1, AIAA,. July 1964.

[31] **Lesieutre, D. J., Love J. F.,** and **Dillenius M. F. E.**
High angle of attack missile aerodynamics including rotational rates - Program M3HAX. AIAA Paper No. 96-3392, 1996, AIAA.

[32] **Kahn, S. D.**, **Oskay, V.** and **Whiteside, J.**,
Verification of Ground Test Data by Instrumented Flight Test of an Artillery Shell.
Journal of Aircraft, Vol.10 No.3, March 1973.

[33] **DeSpirito, J.** and **Heavey, K. R.**,
CFD Computation of Magnus Moment and Roll Damping Moment of a Spinning Projectile
AIAA-2004-4713, AIAA Atmospheric Flight Mechanics Conference and Exhibit, Providence, Rhode Island, August 2004.

[34] **Giraud, M., Berner, C.** and **Winchenbach, G.**,
Aeroballistic Investigation of Supersonic Hemispheric Shapes Computations and Experiments.
ADPA, 16th International Symposium on Ballistics, San Francisco, USA, 1996.

[35] **Moore, F. G., McInville, R. M.** and **Hymer, T. C.,**
Application of the 1998 Version of the Aeroprediction Code.
Journal of Spacecraft and Rockets, vol. 36, no. 5, AIAA, September-October 1999.

[36] **Weinacht, P.** and **Sturek, W. B.,**
Navier-Stokes predictions of static and dynamic aerodynamic derivates for high L/D finned projectiles.
AGARD Conf. Proc., AGARD-CP-493, Paper 20, April 1990.

[37] **Weinacht, P.** and **Sturek, W. B.,**
Computation of the roll characteristics of a finned projectile.
Journal of Spacecraft and Rockets, vol. 33, no. 5, AIAA, November-December 1996.

[38] **Moore, F. G., McInville, R. M.** and **Hymer, T. C.**,
2005 Version of the Aeroprediction Code (AP05).
Journal of Spacecraft and Rockets, March-April 2005, vol. 42, no. 2, AIAA.

INTENTIONALLY BLANK

AEP-4655(A)(1)